*Inorganics* **2014**, *2*, 29-78; doi:10.3390/inorganics2010029

OPEN ACCESS

*inorganics*

**ISSN 2304-6740**

www.mdpi.com/journal/inorganics

*Review*

# Chemistry of Ammonothermal Synthesis

**Theresia M. M. Richter and Rainer Niewa ***

Institut für Anorganische Chemie, Universität Stuttgart, Pfaffenwaldring 55, Stuttgart 70569, Germany; E-Mail: richter@iac.uni-stuttgart.de

* Author to whom correspondence should be addressed; E-Mail: niewa@iac.uni-stuttgart.de; Tel.: +49-711-685-64217; Fax: +49-711-685-64241.

*Received: 10 December 2013; in revised form: 21 January 2014 / Accepted: 27 January 2014 / Published: 28 February 2014*

---

**Abstract:** Ammonothermal synthesis is a method for synthesis and crystal growth suitable for a large range of chemically different materials, such as nitrides (e.g., GaN, AlN), amides (e.g., $LiNH_2$, $Zn(NH_2)_2$), imides (e.g., $Th(NH)_2$), ammoniates (e.g., $Ga(NH_3)_3F_3$, $[Al(NH_3)_6]I_3 \cdot NH_3$) and non-nitrogen compounds like hydroxides, hydrogen sulfides and polychalcogenides (e.g., NaOH, LiHS, CaS, $Cs_2Te_5$). In particular, large scale production of high quality crystals is possible, due to comparatively simple scalability of the experimental set-up. The ammonothermal method is defined as employing a heterogeneous reaction in ammonia as one homogenous fluid close to or in supercritical state. Three types of milieus may be applied during ammonothermal synthesis: ammonobasic, ammononeutral or ammonoacidic, evoked by the used starting materials and mineralizers, strongly influencing the obtained products. There is little known about the dissolution and materials transport processes or the deposition mechanisms during ammonothermal crystal growth. However, the initial results indicate the possible nature of different intermediate species present in the respective milieus.

**Keywords:** high pressure; high temperature; group III nitride semiconductors; ammonothermal synthesis

**Nomenclature:**

| | |
|---|---|
| *A* | Alkali or alkaline-earth metal, *A*(1) = alkali metal, *A*(2) = alkaline-earth metal |
| *B* | Further metal, might be main group metal, transition or rare-earth metal |
| *M* | Transition metal, excluding Sc, Y, La |
| *R* | Rare-earth metal, Sc, Y, La-Lu |
| *X* | Halide |
| *E* | Other main group element |

## 1. Introduction

Ammonothermal synthesis has gained increasing research interest over the last 20 years. The first ammonothermal syntheses were carried out in analogy to the hydrothermal synthesis of oxides in the 1960s by Juza and Jacobs and pursued by Jacobs and co-workers over the following decades [1–3]. Since ammonia resembles water in its physical properties, water was replaced by ammonia in order to obtain amides, imides and nitrides in place of hydroxides and oxides. Using ammonia instead of nitrogen for nitridation allows less harsh temperature and pressure conditions, since ammonia is more reactive. Furthermore, an abundance of further materials like hydroxides, chalcogenides and hydrogen sulfides can be also obtained from supercritical ammonia.

Both hydrothermal and ammonothermal synthesis are part of the large group of solvothermal methods. The use of the term solvothermal is not defined unambiguously. Definitions vary from "*any heterogenous chemical reaction in the presence of a solvent (whether aqueous or non-aqueous) above room temperature and at pressure greater than 1 atm in a closed system*" [4] to sub- or supercritical conditions of the solvent [5]. Rabenau's definition for hydrothermal conditions is frequently used "*an aqueous medium over 100 C and 1 bar*" [6] and transferred to solvothermal conditions in general by adjusting 373 K to "*the boiling point of the solvent*" [7]. The characteristics of ammonothermal synthesis and its products are mainly influenced by high pressure and temperature and usually syntheses are carried out under supercritial conditions. Above the critical point, solvents exist as homogeneous supercritical fluids, where gas and liquid phase can no more be distinguished and consequently the properties of the different phases converge. However, the properties of a supercritical fluid in its proper meaning and those of a fluid, with only one physical quantity above the critical state and the other one slightly below it, are hardly distinguishable. Hence, we define ammonothermal synthesis as a reaction in ammonia as one homogenous fluid next to or under supercritical conditions.

Various solvents showing distinct different chemical properties are used for solvothermal syntheses. This comprises (i) polar protic solvents like $H_2O$, $NH_3$, HF, HCl, HBr; (ii) polar non-protic solvents like tetrahydrofuran and (iii) non-polar solvents like benzene, xylene and $CO_2$. Table 1 gives some examples for solvents used in solvothermal techniques and the obtained products. Over recent years, the research interest in solvothermal methods has greatly increased, due the constantly raising demand of crystal growth of functional materials, like, for example, semiconductors ($CuInSe_2$ [8], InAs [9], GaN [10], AlN [11] and ZnO [12]), piezoelectrics ($\alpha$-quartz [13], $GaPO_4$ [14]), electrodes for lithium batteries

($Li_{1-x}Mn_2O_{4-y}$ [15]), magnetic and catalytic materials ($La_{1-x}Ca/Sr/BaMnO_3$ [16]) and fine dielectric ceramics ($BaTiO_3$ [17]).

**Table 1.** Examples for solvothermal solvents and obtained products (see text).

| | Solvent | Examples for products | References |
|---|---|---|---|
| (i) | $H_2O$ | ZnO, $\alpha$-quartz, $\alpha$-$Al_2O_3$, $GaPO_4$ | [12–14,18] |
| | $H_2O$ + isopropyl alcohol | $BaTiO_3$ | [17] |
| | $H_2O$ + $C_2H_3Cl_3$ | Diamond | [19] |
| | $NH_3$ | GaN, AlN, $Cu_3N$, $Cs_2S_2$, NaOH | [10,11,20–22] |
| | HCl, HBr, HI | BiSCl, BiTeBr, SbSeI | [23] |
| | Ethanol | $Li_{1-x}Mn_2O_{4-y}$ | [15] |
| | Benzyl alcohol | $La_{1-x}Ca/Sr/BaMnO_3$ | [16] |
| (ii) | Ethylendiamine | $Cu_7Te_4$, $CuInSe_2$ | [8,24] |
| | Diethylamine | $CuInSe_2$ | [8] |
| | THF | β-MnS | [25] |
| (iii) | $C_6H_6$ | Se, *c/h*-BN, $\gamma$-MnS | [25,26] |
| | Xylene | InAs | [9] |
| | Toluene | $CuCr_2Se_4$ | [27] |
| | $CO_2$ | Poly vinyl chloride | [28] |
| | $Br_2$ | SbSBr | [23] |

The choice of the solvent considerably influences the obtained product. Even different modifications occur depending on the solvent. For the reaction of $MnCl_2 \cdot 4\,H_2O$ with thiourea, $SC(NH_2)_2$, to MnS, for example, the use of tetrahydrofuran (THF) as solvent leads to metastable β-MnS, with benzene as solvent exclusively metastable $\gamma$-MnS and with water or ethylenediamine the stable $\alpha$-MnS occur. Thus, the crystallization of the different modifications depends on the formed complexes of the solvent with the substrate, e.g., $[Mn(H_2O)_6]^{2+}$. The knowledge of the chemical nature of the dissolved species is the crucial information to understand the formation mechanism of MnS [25]. Those observations manifest the importance of the complex intermediates present in the solvent for the formed product and for the structure of the product.

The best explored solvothermal method is the hydrothermal synthesis, owing to its commercial application for the synthesis of oxides and hydroxides. Nowadays, the hydrothermal method is used, for example, in the industrial synthesis of over 3000 t $\alpha$-quartz single crystals per year, due to their piezoelectric properties and of $Al_2O_3$ from more than 90 million t of bauxite per year, for processing to metal [4].

Already in 1839, Bunsen carried out experiments with liquids at high temperatures and high pressures (473 K, 150 MPa) [29]. For this purpose he used sealed glass tubes with integrated mercury manometer. Later, in 1848, he succeeded in the growth of $BaCO_3$ and $SrCO_3$ millimeter-long crystals from an aqueous solution at 473 K and 1.52 MPa using $NH_4Cl$ as mineralizer [30]. Similar experiments for recrystallization of apophyllites were apparently conducted by Wöhler earlier [30]. Already in 1845 Schafhäutl obtained for the first time micro crystalline quartz crystals from hydrothermal conditions [31].

In 1851 Sénarmont laid the foundation for hydrothermal mechanisms in geology. He already realized the importance of pressure and temperature *...pressure to maintain the gaseous reactants in a forced dissolution and temperature to favorite certain combinations or decompositions...* for the formation of the minerals and synthesized a great number of natural minerals under high temperature and high pressure conditions, in order to elucidate the natural formation conditions. Using a similar experimental setup as Bunsen did, he applied high temperatures and high pressures in sealed glass tubes. To avoid explosion of the sealed glass tubes containing the reactants and the solvent (water), he placed them inside water filled autoclaves [32].

The ammonothermal method was established inter alia in order to synthesize high quality crystals of amides for XRD structure determination and of deuteroamides for neutron diffraction [3]. The first compounds obtained from ammonothermal conditions (up to 507 MPa and 823 K) were binary amides ($Be(NH_2)_2$, $Mg(NH_2)_2$ [2]) and binary nitrides ($Be_3N_2$ [1]), later also imides ($Th(NH)_2$ [33]), ternary compounds and other than nitrogen containing materials were synthesized [3].

Over the last twenty years the research interest in the ammonothermal method has increased considerably, since it is one of the few techniques leading to group III bulk nitrides. In comparison to other techniques, the ammonothermal method allows crystal growth on native substrate and growth of the initial native substrate itself in a very high quality. Increasing commercial efforts are directed to the ammonothermal growth of GaN and AlN on native substrates. GaN and AlN are semiconductors with wide band gaps used as base for optoelectronic and electronic devices (e.g., light-emitting diodes (LEDs), high electron mobility transistors, lasers with high optical storage capacity). The growth of group III nitrides as bulk crystal is much more difficult than as micro crystalline powder, but necessary for the use in optoelectronic and electronic devices [34,35].

There are several other methods known for the synthesis of bulk GaN and AlN. Up to now the most popular technique is hydride or halide vapor phase epitaxy, which is used for commercial purposes. Vapor-phase GaCl or $GaCl_3$ obtained from metallic Ga and gaseous HCl is carried in a gas flow and reacts with gaseous $NH_3$ to form GaN. The formed GaN deposits usually on a non-native substrate like sapphire, silicon or GaAs. At ambient pressure, growth temperatures of 1000–1100 °C are typical and growth rates of up to 0.5 mm/h are reported. Wafers are cut from the formed bulk material and subsequently polished. They can be used in devices or as a substrate for further syntheses [36].

Metal organic vapor phase epitaxy allows the growth of thin epitaxial layers used for devices. Metalorganic precursors (e.g., triethyl or trimethyl-gallium) react with $NH_3$ forming GaN on a substrate. Growth rates vary from 1–2 μm/h for thin layers and up to 50 μm/h for bulk growth [36].

The advantages of devices made from ammonothermal GaN are the lower defect, strain and bowing level due to the growth on native substrate, the possibility of high scalability and no tilt boundaries, which occur even at GaN grown on a native seed by hydride/halide vapor phase epitaxy. If the substrate shows tilt boundaries, even if it is a native substrate but grown itself on a foreign substrate, the tilt boundaries will appear in the grown material, too [10,37–42]. High quality of the substrate is very important, since it allows the production of more devices per substrate and devices made of low-defect-density GaN or AlN promise longer working periods at higher power without breakdown [43]. Solvothermal methods in general are known for their reliable and scalable process, which permits the efficient growth of a great number of crystals within one synthesis, e.g., 1400 quartz crystals, 1700 g each [36,44].

Slow growth rates were one of the disadvantages of the ammonothermal method in the past. According to the latest research results this problem seems to overcome. Recently, researchers increased growth rates for GaN by ammonothermal method from 24–106 µm/d [45] to 250 (*c*-plane) and 300 µm/d (*m*-plane) in the presence of $NH_4F$, used as so-called mineralizer [46]. Even *m*-plane growth rates of up to 40 µm/h (=960 µm/d) with rates of 10–30 µm/h (=240–720 µm/d) for all planes were reported recently [39].

## 2. Ammonia as Solvent

Ammonia and water show quite similar properties (see Table 2). Hence, the parallel from supercritical water to supercritical ammonia, drawn and realized by Juza and Jacobs, who established the ammonothermal synthesis, is not surprising [1,2]. Ammonia is a non-aqueous ionizing solvent, that means pure ammonia has a low specific electrical conductivity and dissolved electrolytes are partially or completely dissociated [47]. Ammonia was the first ionizing solvent, except for water, which has been studied thoroughly. Already at the beginning of the 20th century, inter alia Franklin, Kraus and Bronn studied the ammono-system of compounds, e.g., metal solutions in liquid ammonia [48–50]. Still, supercritical and liquid ammonia is a far less explored solvent than water. Compared to water ammonia is less protic and polar, at ambient pressure and temperature it is gaseous and shows much higher pressures at high temperatures [51]. Liquid ammonia has only small solubilities for many inorganic compounds, which yields often poorly crystallized or amorphous solids on precipitation, due to inhibited nucleation and crystal growth. Using supercritical ammonia rather than liquid ammonia overcomes this problem: Under ammonothermal conditions (supercritical fluid above a pressure of 11.3 MPa and a temperature of 405.2 K [52] see Figures 1 and 2 [53]) the solubility is high enough to dissolve a large number of inorganic compounds. To dissolve a solid the relative permittivity of the solvent has to be higher than the lattice energy of the solid. Due to the rising relative permittivity of solvents with increasing density, which occurs at higher pressure, the solubility of mostly ionic solids increases with increasing pressure [3,54]. Water has a higher relative permittivity than ammonia; therefore, solids dissolve better in water than in ammonia at similar conditions (see Table 2).

**Table 2.** Comparison of selected properties of ammonia and water [47,52,55].

| | **Water** | **Ammonia** |
|---|---|---|
| $T_{\text{crit.}}$/K | 647.65 | 405.2 |
| $p_{\text{crit.}}$/MPa | 22.1 | 11.3 |
| $\epsilon_r$ | 78.3 (298 K) | 16.9 (298 K) |
| Autoprotolysis | $2H_2O \rightleftarrows H_3O^+ + OH^-$ | $2NH_3 \rightleftarrows NH_4^+ + NH_2^-$ |
| Ionic product | $10^{-14}$ (298 K) | $10^{-32}$ (239 K) |
| $pk_B$ | 15.7 | 4.75 |
| Proton affinity/eV | −7.9 | −9.2 |

Ammonia has a higher proton affinity than water ($E_{pa}(NH_3)$ = –9.2 eV; $E_{pa}(H_2O)$ = –7.9 eV [47]; the energy released when a proton is attached to the molecule in the gas phase). Hence, ammonia is

a more basic solvent than water (see $pk_B(NH_3)$ = 4.8 and $pk_B(H_2O)$ = 15.7 [47]). Both water and ammonia show autoprotolysis since they possess at least one non-bonding pair of electrons and acidic hydrogen atoms, leading to formation of $H_3O^+$ or $NH_4^+$ cations and $OH^-$ or $NH_2^-$ anions, respectively. Due to the endothermic nature of the autoprotolysis reactions, the magnitude of autoprotolysis increases with increasing temperature. In the same way as water is a suitable solvent for the synthesis of oxides, ammonia is a unique and excellent solvent for nitride synthesis. Additionally, liquid and supercritical ammonia find application as solvent for water sensible compounds, which do not necessarily contain nitrogen, e.g., sulfides, hydrogen sulfides [3,56,57] and hydroxides [22].

**Figure 1.** Pressure-temperature phase diagram of ammonia. The dashed line is extrapolated [58].

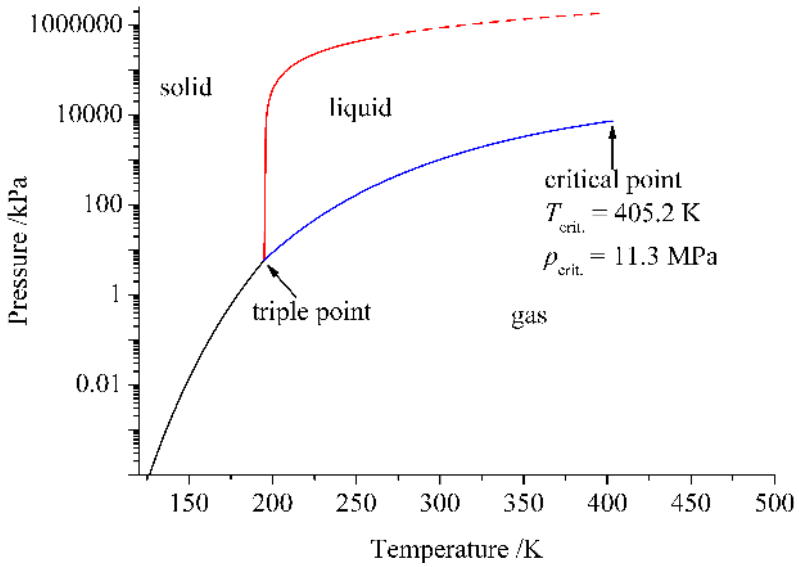


**Figure 2.** Pressure-temperature diagram of ammonia in dependence on the filling degree of the reaction vessel (in %). The inset shows an enlarged view in the range around the critical point ($T_{crit.}$ 405.2 K, $p_{crit.}$ = 11.3 K) [53].

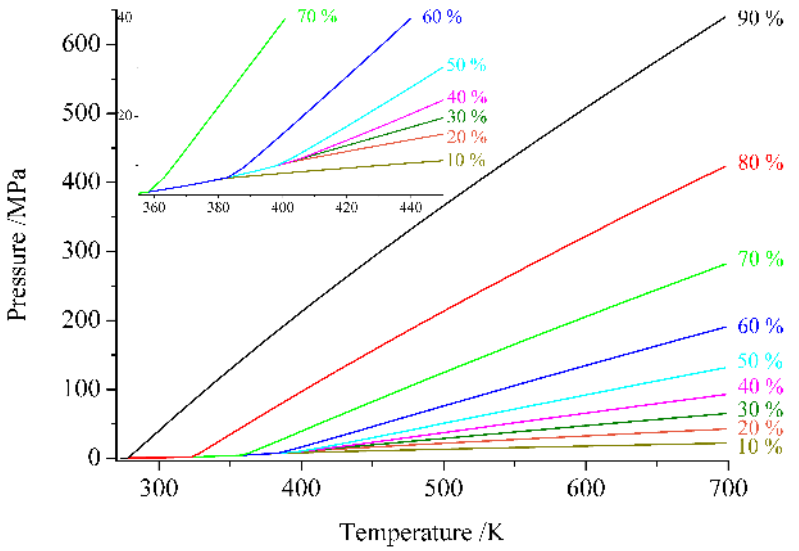

## 3. Technical Details for Ammonothermal Reactions

There are different installations for the realization of ammonothermal synthesis, starting with the materials and construction of the reaction vessel, the inner shape, liner and geometry of the reaction vessel via the filling of the reaction vessel with ammonia to the heating of the reaction vessel. In general, two types of ammonothermal syntheses can be distinguished, covering different aims: the research on fundamental questions and the research on application of the method for crystal growth. The former research branch investigates new compounds, new synthesis routes for compounds and the processes during crystal growth. The latter investigates and applies the conditions for an optimal crystal growth, including low defect and crack concentration, high growth rates and large crystal size, aiming at a commercial application. The different objectives require different laboratory installations, not only of size but also of type.

The reaction vessel is referred to as autoclave, since most of the installations use steel autoclaves and even the techniques with metallic capsules and glass tubes as reaction containers usually use steel autoclaves for mechanical stabilization of the capsule.

**Figure 3.** Flow chart of an ammonothermal reaction setup for the simultaneous pressure and temperature control during reaction using two pumps. The heat exchanger is used for pre-cooling one pump and the supply pipe [59,60].

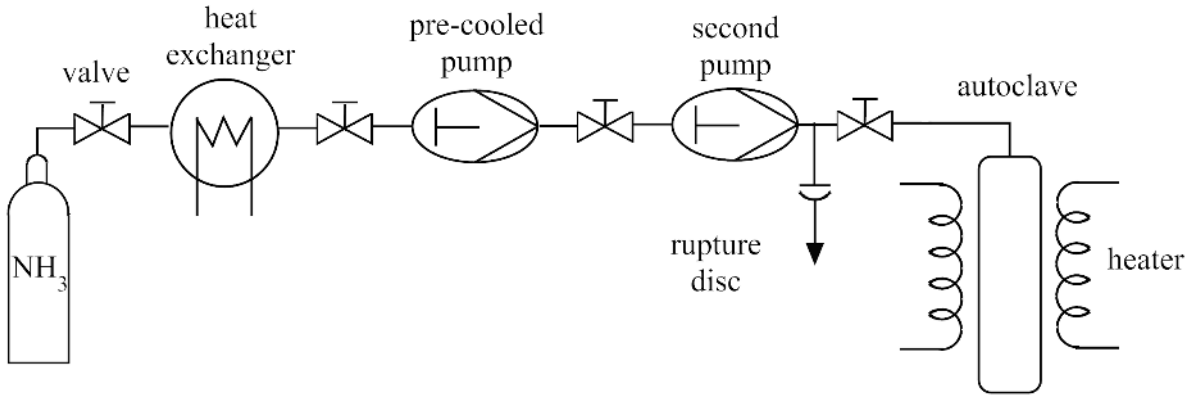


Different approaches find application to fill the autoclave with ammonia: Condensing ammonia into the autoclave by cooling, adding solid ammonia or filling the autoclave sequentially with ammonia by high pressure pumps. Condensing ammonia into the autoclave historically is realized by the help of a tensieudiometer, an apparatus for the simultaneous measurement of pressure and volume, developed by Hüttig [61]. The autoclave, already loaded with the solid reactants, can be connected to the tensieudiometer and is cooled down below the boiling point of ammonia ($T \leq 239.79$ K at ambient pressure [52]) and ammonia condenses in the autoclave. Since volume and pressure in the tensieudiometer, which realizes a closed system including the autoclave, are known an exact amount of ammonia can be filled inside the autoclave. To cool the autoclave down, usually the autoclave body is placed in a cooling bath of acetone or ethanol and dry ice. Adding solid ammonia, solidified by cooling in liquid nitrogen is an other option, which is necessary if glass tubes are used, since the glass tubes are sealed at high temperatures after filling. Liquid ammonia would evaporate too fast at those temperatures. Both filling methods only allow limited control of the pressure during synthesis, by the amount of added

ammonia before the synthesis and the applied temperature during synthesis. Pressure control during synthesis is possible using high pressure pumps, which compress ammonia prior to reaction and control the pressure during synthesis. A system of two high pressure pumps with a pre-cooled compressor and supply pipe (258–263 K) guarantees the condensation of the gaseous ammonia, using only one pump allows the system to reach pressures of 5–30 MPa, since the pressure increases with increasing temperature (see Figure 3). The use of a second pump permits the variation of the pressure during synthesis and pressures of up to 450 MPa [3,59,60].

Concerning the temperature at least two different temperature zones inside the reaction chamber have to be achieved in order to obtain a temperature gradient. The temperature gradient contributes via convection to the mass transport of the dissolved species during synthesis and is essential for the crystallization process (see section *Crystallization Process*). The temperature gradient can be applied by different heaters around or integrated into the autoclave, by not heating or even cooling one part of the autoclave. Autoclave models with integrated cooling were also reported, see Figure 4 [3,39].

**Figure 4.** Flow chart of an ammonothermal autoclave with integrated cooling and external heating [3].

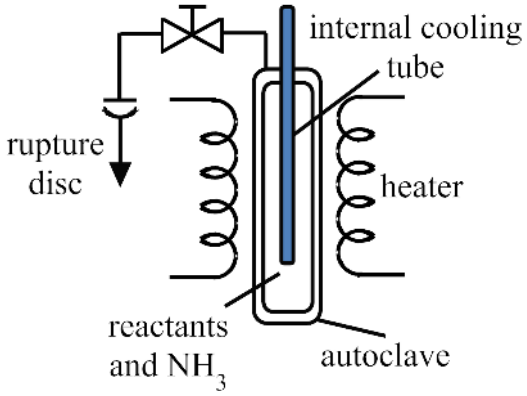


### *3.1. Reaction Vessels*

The first reaction vessels for supercritical syntheses were sealed thick-walled glass tubes with integrated mercury manometer, which withstand temperatures of up to 473 K and pressures of up to 15 MPa [29]. Sénarmont was the first to apply a counter-pressure to avoid explosion of the sealed glass tubes containing the reactants, by placing them inside water filled autoclaves [32]. Similar counter pressure systems are still in use for ammonothermal synthesis. Sealed glass, silver or gold ampoules are used as reaction vessels for ammonothermal synthesis, containing the starting materials and supercritical ammonia. To avoid explosion, the ampoules are placed in a steel autoclave, connected to a high pressure pump, which produces a counter-pressure of nitrogen inside the autoclave (see Figure 5). The counter-pressure should only be slightly lower than the pressure inside the ampoule. However, in order to simplify the handling the counter-pressure is usually higher than the pressure inside the ampoule. For supercritical conditions, the autoclave containing the ampoule is placed in a heater. In this way, pressures and temperatures of up to 280 MPa and 470 K for glass ampoules are realized, metal ampoules enable the application of higher temperatures [3]. Recently, a similar construction was used for large scale

GaN crystal growth in a vessel with internal heating. The reaction is carried out in a welded capsule, containing the starting materials and supercritical ammonia. The capsule is coated directly by a heater, followed by a ceramic shell and an externally-cooled steel shell. The inner heater reaches temperatures of up to 1023 K at 600 MPa, while the temperature of the outer steel shell remains below 473 K, due to the insulating ceramic shell. The use of an internal heating allows the application of higher temperatures and higher pressures compared to autoclaves made of nickel based superalloys, additionally the use of conventional steel is less expensive in production and processing [39]. Nickel based superalloys, for example, Inconel 750 [6], Vacumelt ATS 340 [3], Inconel 718 [59] and Rene 41 [36] are used for the construction of high pressure autoclaves with external heating. Those superalloys almost resist corrosion in ammonobasic milieu up to temperatures of ~873 K at ≥3000 MPa (Inconel 750) and can stand even ≤1123 K at ≤150 MPa (Rene 41) [62]. Autoclaves made of those alloys are loaded directly with the starting materials and ammonia and are heated up with an external direct heater. This explains the milder working conditions.

**Figure 5.** Flow chart of an ammonothermal reaction setup using a glass or metal ampoule filled with ammonia and the reactants placed in a steel autoclave connected to a high pressure pump, applying a counter-pressure of nitrogen [3].

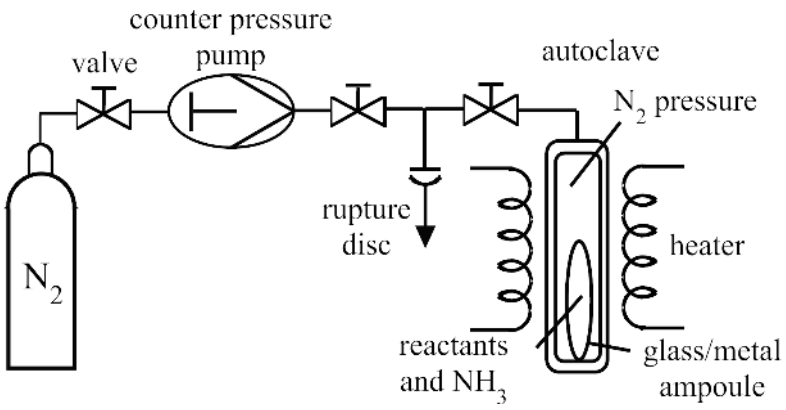


Depending on the reaction conditions, the use of a liner may be necessary. Ammonobasic conditions are usually less corrosive than ammonoacidic conditions. Thus, a nickel based superalloy as autoclave material is often sufficient. However, in ammonobasic conditions, nickel based alloys can also be affected and a supplementary liner can be useful. We have observed the formation of nickel compounds from the autoclave material at $T \geq 840$ K with zinc or gallium as reactant. Indium metal used as reactant passed the autoclave material by diffusion along the grain boundaries and leads to the destruction of the autoclave. For ammonoacidic conditions, liners are used to protect the products from metal impurities originating from the autoclave material. Especially chromium and nickel impurities in the compounds or even chromium and nickel based compounds are observed. Precious metals are used as liner materials, particularly silver, gold and platinum, although the choice of liner material restricts the choice of the mineralizer. However, the formation of a nitride layer on the surface of the autoclave material at $T \sim 800$ K in supercritical ammonia during synthesis, resulting in a hard surface of nitrides, seems to protect the autoclave material in some cases to a certain amount from corrosion [3].

According to the use of the autoclave, the inner geometry is constructed differently. Ammonothermal syntheses on a fundamental research level, investigating new compounds, synthesis routes and processes do not obligatory require special inner shapes of the autoclave. Only the starting materials, including mineralizer, are loaded into the autoclave in one of the two temperature zones, subsequently the formed products, the crystallization spot and the dependence on temperature and pressure are investigated. However, ammonothermal syntheses exploring the crystal growth usually use seed crystals and a feedstock of micro crystalline powder, both containing the same metal (mostly GaN or AlN but also metal amides, metal halides or pure metal) and placed in different temperature zones of the reaction vessel. The micro crystalline powder is diluted with the help of a mineralizer and transported to the seed crystals, where it deposits. In this way, large crystals are obtained. The epitaxial growth on the seed crystal can be heteroepitaxial on foreign substrate or homoepitaxial on native substrate. This method is suitable for large scale commercial synthesis of AlN and GaN [63]. Often a baffle is used, in order to optimize the heat and mass transport inside the autoclave, since it is capable of controlling the flow pattern in the system. Different baffle designs are used, depending on the transport direction in the system.

## 4. Crystallization Process

The ammonothermal synthesis corresponds, in its thermodynamical fundaments and many chemical aspects, to the well studied Chemical Vapor Transport. The definition of the Chemical Vapor Transport by Binnewies *et al.* applies on a fundamental level: "textita condensed phase, typically a solid, is volatilized in the presence of a [...] transport agent, and deposits elsewhere, usually in the form of crystals" [64]. For the ammonothermal method this means: A solid phase is dissolved in supercritical ammonia initiated by chemical reaction with the added mineralizer forming complex ions, the complex ions are transported into the crystallization zone and deposit there under reformation of the solid as micro crystalline powder or single crystals. Crucial for the transport is the solubility of the compound ($\geq$3% [65]) and the presence of a gradient. In principle, the gradient may concern any state variable leading to a difference in solubility. Typically, temperature gradients are used in crystal growth due the most simple realization by applying two or more different heaters realizing different temperatures and consequently producing two or more different temperature zones inside the reaction vessel.

There are currently many research efforts in maximizing growth rates and crystal sizes and in minimizing defects and strain/bowing levels. However, there appears only very little work done in order to understand the reasons for the achieved improvements. Knowledge and understanding of the physical and chemical processes during ammonothermal crystal growth allows a controlled and efficient improvement of the crystal growth process. Due to the influence of various parameters, this process is very complex. Two groups of parameters can be distinguished: Chemical parameters like the solvent, the chemical nature and the concentration of nutrient and mineralizer, and thermodynamical parameters like the pressure, the temperature in dissolution and crystallization zone and the temperature gradient contribute to the crystal growth [5]. Over the last years, there have been some initial studies carried out clarifying the processes during ammonothermal synthesis and especially the formation mechanism of GaN from supercritical ammonia. The research efforts cover different points of both groups of

parameters, yet the influence of most parameters are not well examined and require further intense research efforts.

By isolation of intermediate compounds, evaluation of crystallization and dissolution zone, and determination of solubility of Ga species, important information for the formation mechanism of GaN from supercritical ammonia are obtained. Additionally, spectroscopic data of the intermediate compounds were collected representing the base for future *in-situ* measurements for further exploration of the GaN formation mechanism [66,67]. Special optical cells for *in-situ* monitoring during ammonothermal process were developed [59,60,68]. A combination of the *in-situ* monitoring technology and preliminary work on intermediate compounds allows to obtain further information for a complete unravelment of the ammonothermal synthesis. In order to understand the role of applied temperature, temperature gradient and baffle design for an optimized transport and consequently for the crystal growth first theoretical 3-D simulations for the ammonothermal process were furnished, revealing a strong dependence of the flow pattern by the baffle shape. A positive inclination of the baffle leads to an upward directed jet stream through the baffle opening and vice versa. The baffle shape not only influences the flow pattern but also the temperature profile. These information may be used to control specifically the crystallization and the mass transport from dissolution to crystallization zone, and to avoid parasitic crystal growth [69].

### *4.1. Thermodynamical Parameters*

Knowledge about thermodynamical parameters (temperatures, pressure and reaction time) during ammonothermal crystal growth is crucial to adjust the growth conditions. High pressure allows us to decrease the temperature so that comparatively mild conditions can be applied. Depending on the desired product, temperature and pressure have to be adapted. In general, high temperature and low pressure favors the formation of binary nitrides and low temperatures and high pressures the stabilization of ternary amides, ternary ammoniates or mixed ternary compounds. Regarding the temperature, different aspects have to be respected: the dissolution temperature, the growth temperature and the temperature gradient. Generally speaking, increasing temperature and pressure yields a higher solubility of the starting materials, but the nature of the reactants and the products' solubility (negative or positive temperature dependance) have to be considered. For the transport of the mobile species, a gradient, typically in temperature, is necessary, determining the transport of the mobile species in solution and the kinetics. The transport can be performed dominated by convection or by diffusion, with convection by a gradient being much faster. A vertical gradient, typically meaning a vertical position of the reaction vessel, favors the transport via convection, while a horizontal position minimizes almost entirely the transport to diffusion, which leads to much slower transport rates. However, higher transport rates often yields higher defect densities. Thus, the kinetics have to be adapted according to the advantages of a high growth rate and the disadvantages of increased defect densities [5,7]. A temperature gradient can easily be applied by different heaters, by the lack of a heater on some parts of the reaction vessel or by an induced cooling.

The influence of the thermal decomposition of ammonia obeying reaction Equation (1) during ammonothermal synthesis at temperatures up to 873 K is expected to be small. $H_2$ formed from the dissociation or as by-product of chemical reactions during dissolution or recrystallization has been shown

to diffuse through the autoclave wall [3,70]. Jacobs and Schmidt concluded that equilibrium Equation (1) has to lie more on the left side, as they could not detect any $N_2$ after reaction and their autoclaves would not have stand pressures as high as the extrapolated values [3].

$$2\ NH_3 \rightleftarrows N_2 + 3\ H_2 \tag{1}$$

### *4.2. Chemical Parameters*

Chemical parameters have previously been studied for solvothermal methods using other solvents than ammonia. We will limit ourselves to few examples: For the basic hydrothermal synthesis of wurtzite-type ZnO (starting materials: $Zn(NO_3)_{2(aq)}$, $NH_4OH$ in $H_2O$ at ambient pressure and 373 K) the mechanism starts with dissolution of the ZnO nutrient by means of a mineralizer forming different soluble intermediate species $[ZnOOH]^-$, $[Zn(OH)_4]^{2-}$ and $[ZnO_2]^{2-}$, which occur in different concentrations depending on $OH^-$ concentration and temperature and the solid $\epsilon$-$Zn(OH)_2$, which crystallizes as solid intermediate [44]. *h*-ZnO was shown to form via the crystalline intermediate $\epsilon$-$Zn(OH)_2$, where the conversion takes place interior solid $\epsilon$-$Zn(OH)_2$. Simultaneously, on the outer surface layers exposed to the solution, *h*-ZnO is formed directly from $\epsilon$-$Zn(OH)_2$, or exchanged with solution. $\epsilon$-$Zn(OH)_2$ crystallizes from soluble species ($[Zn(OH)_{4-n}(H_2O)_n]^{2-n}$; $n = 0, 1$) [12]. A possible ZnO formation mechanism for the growth on a ZnO seed crystal is shown in reaction Equation (2), while reaction Equation (3) shows the solid-solid transformation from spontaneously nucleated $\epsilon$-$Zn(OH)_2$ to *h*-ZnO.

$$\begin{aligned} ZnO\ (nutrient) + 2\ OH^- + H_2O \rightleftarrows [Zn(OH)_4]^{2-} \rightleftarrows Zn(OH)_2 + 2\ OH^- \\ \rightleftarrows [ZnO_2]^{2-} + 2\ H_2O \rightleftarrows ZnO\ (crystal) + 2\ OH^- + H_2O \end{aligned} \tag{2}$$

$$Zn(OH)_2 \rightleftarrows ZnO + H_2O \tag{3}$$

Extensive research has also been done on the mechanism during hydrothermal growth of zeolites. It has been shown, e.g., that the dissolved species taking part in the crystallization process are small and of simple structure. The growth from larger and more complex species is too time consuming and has a higher defect probability due to different docking possibilities on the crystal surface. A high defect concentration may slow down or even entirely stop the crystal growth [71]. $[Si(OH)_3O]^-$ and $[Al(OH)_4]^-$ monomers are taken to represent the building species in zeolite crystal growth [71,72].

During ammonothermal synthesis, various ionic species may occur. The nature of these species is strongly related to the acidity of the system. Three types of milieus arise, evoked by the used starting materials: ammonoacidic ($NH_4^+$ present), ammononeutral (e.g., $NO_3^{2-}$ present) and ammonobasic ($NH_2^-$ present). The milieu determining ions ($NH_4^+$ and $NH_2^-$) derive from the acidic or basic mineralizer and the autoprotolysis of ammonia. Mineralizers added to the reactants are applied to establish a defined milieu. Sometimes a tiny amount of a co-mineralizer (e.g., alkali metal halides) is added to activate the reaction. Although the role of mineralizers in chemical reactions is not always known, they are used in ammonothermal synthesis [66,67] as well as in various further methods (gas phase transport reactions [64], hydrothermal synthesis [4], synthesis in liquid ammonia [54,73,74]). Similar applies to the so-called co-mineralizers. The mineralizers fulfill different functions in the growth process: to convey the solubility of the starting material by inducing the formation of soluble and consequently

mobile species, to enable and enhance the formation of new chemical bonds and compounds, and finally to detach from the desired compound to be able to act like a catalyst (especially in case of growth of binary compounds). The importance of the choice of the mineralizer can be seen in the fact that they determine the transportation direction of the product in the gradient within the autoclave (see paragraph *Intermediate Species controlling Solubility and Growth Rates*).

#### 4.2.1. Ammonobasic Systems

Typically, alkali metal amides $A(1)NH_2$, alkali metals or alkali metal azides are use as ammonobasic mineralizers. Ammonia reacts with alkali metals and alkali metal azides according to reactions Equations (4) and (5) to form $NH_2^-$, such that the solution turns basic. The same applies for alkaline-earth metals and some rare-earth metals. However, alkali metal amides and azides are easier to handle due to their powder shape and lower reactivity compared to the metal bulk material. Alkali metal amides are favorable if no formation of hydrogen or additional nitrogen pressure is desired.

$$2\ NH_3 + 2\ A(1) \rightarrow 2\ NH_2^- + H_2 + 2\ A(1)^+ \tag{4}$$

$$2\ NH_3 + 3\ N_3^- \rightarrow 3\ NH_2^- + 4\ N_2 \tag{5}$$

During ammonothermal synthesis, in analogy to the experience from hydrothermal research, it is expected that the metal dissolves by help of the mineralizer, forming intermediate species of the type $[B(NH_2)_n]^{m-}$, possibly also as complex imides or amide imides. Those complex anions are transported in the supercritical ammonia from the dissolution to the crystallization zone, where the crystallization takes place.

Ammonobasic mineralizers like $KNH_2$ are known from syntheses of binary metal amides in liquid ammonia for a long time. The latter binary amides are formed from metal salt solutions in liquid ammonia with $KNH_2$ as a little soluble precipitate. An example for this synthesis is the formation of $Cd(NH_2)_2$ from $Cd(SCN)_2$ in liquid ammonia with $KNH_2$ as mineralizer. The application of alkali metal amides as mineralizers only work, if there are no ternary alkali metal amides formed. Often with small amounts of mineralizer binary amides, with large amounts ternary amides are obtained. Beryllium and zinc always form ternary amides [74].

There is a large number of ternary amides of two metals synthesized in supercritical ammonia from the metals (see paragraph *Ternary Amides*) at comparatively high pressures and low temperatures. Ternary amides decompose to imides and further to nitrides, under release of ammonia. Before the formation of pure nitrides is completed, metal hydrides and mixed hydride nitrides may be obtained as shown in the systems Th/H/N [33], Zr/H/N [75] and Ce/H/N [76], especially at temperatures below the formation temperature for pure nitrides.

It is also known that various bulk binary nitrides are formed from the metal in supercritical ammonia using an ammonobasic mineralizer (see paragraph *Nitrides*), from technological point of view, the most interesting examples currently being the semiconductors GaN [77] and AlN [78]. Recent research in ammonobasic conditions indicates that the binary nitrides are formed via ternary amides functioning as intermediate species [67,79] following the assumed reaction Equation (6). $K[Ga(NH_2)_4]$ and $Na[Ga(NH_2)_4]$ convert to *h*-GaN at higher temperatures [80,81]. For GaN synthesis from Ga

with $LiNH_2$ in supercritical ammonia, $Li[Ga(NH_2)_4]$ was proposed as possible intermediate compound [79] and was indeed recently found to crystallize in two modifications in the hot zone of the autoclave [67]. In the system Ga/Na/$NH_3$ two ternary amides are known, namely $Na[Ga(NH_2)_4]$ [81] and $Na_2[Ga(NH_2)_4]NH_2$ [67,82] to form under ammonothermal conditions. The former predominates at high pressures, whereas the latter is obtained mainly at lower pressures. With potassium only one solid compound $K[Ga(NH_2)_4]$ [80] and an intriguing liquid "$KGa(NH)_n \cdot xNH_3$" were reported [65]. Decomposition of $Na[Al(NH_2)_4]$ under release of ammonia at temperatures below 373 K is known to proceed via a liquid compound. An intermediate "$NaAl(NH_2)_2(NH)$" was proposed according to volumetric measurements of released ammonia. Further heating leads to a mixture of AlN and $NaNH_2$ [81]. Knowledge about those intermediate compounds is not only interesting for the formation mechanism, but also for understanding the temperature dependance of the solubility of GaN in supercritical ammonia.

$$A(1)_nGa(NH_2)_{3+n} \rightleftarrows GaN + nA(1)NH_2 + 2NH_3 \tag{6}$$

4.2.2. Ammonoacidic Systems

Ammonothermal synthesis in ammonoacidic milieu is a powerful method to obtain ammoniates, nitrides and even amides. The effect of ammonacidic milieu is due to the presence and increased concentration of ammonium ions $NH_4^+$. Ammonoacidic milieu is well known from syntheses in liquid ammonia [54,73], where, e.g., $NH_4I$ is used as ammonoacidic catalyst for the precipitation of $Mg(NH_2)_2$ from magnesium according to the following reaction [73]:

$$\begin{aligned} Mg + 2\ NH_4^+ &\rightleftarrows Mg^{2+} + 2\ NH_3 + H_2 \\ Mg^{2+} + 4\ NH_3 &\rightleftarrows Mg(NH_2)_2 + 2\ NH_4^+ \end{aligned} \tag{7}$$

Typical ammonoacidic mineralizers comprise ammonium halides $NH_4X$ ($X$ = F, Cl, Br, I) and metal halides $BX_n$ ($X$ = F, Cl, Br, I; $B$ = for example, Al, Ga, Fe, Zn).

Several aluminum halide ammoniates are known $[Al(NH_3)_5X]X_2$ ($X$ = F [83], Cl, Br, I [84]), obtained from different synthetic approaches. Ammoniates of aluminum halides are supposed to represent intermediate compounds in the ammonoacidic AlN synthesis. Analogously, there are ammoniates from gallium halides with different amounts of ammonia molecules per gallium kown. In GaN hydride or halide vapor phase epitaxy these occur as volatile precursors, accomplishing the gallium transport to the crystallization zone.

In liquid ammonia gallium halides form hexammoniates such as $[Ga(NH_3)_6]Br_3 \cdot NH_3$ and $[Ga(NH_3)_6]I_3 \cdot NH_3$ [66,85]. Those ammoniates contain octahedrally surrounded $Ga^{3+}$ forming positively charged complex ions $[Ga(NH_3)_6]^{3+}$, which may represent the mobile Ga-containing species in solution. At higher temperature and pressure gallium metal reacts with ammonium halides $NH_4x$ ($X$ = F, Cl) to the ammoniates $[Ga(NH_3)_5Cl]Cl_2$ or $Ga(NH_3)_3F_3$ and GaN [66]. Obtaining $[Ga(NH_3)_5Cl]Cl_2$ and $Ga(NH_3)_3F_3$ during ammonothermal crystal growth of GaN next to GaN confirms the assumption of their role as intermediate species in the GaN synthesis from supercritical ammonia. $[Ga(NH_3)_5Cl]Cl_2$ contains octahedral units $[Ga(NH_3)_5Cl]^{2+}$, which may again represent the Ga-transporting species in solution. In solid $Ga(NH_3)_3F_3$ gallium occurs in two different species, namely $[Ga(NH_3)_4F_2]^+$ and $[Ga(NH_3)_2F_4]^-$.

Thus, in solution cationic $[Ga(NH_3)_4F_2]^+$ and anionic $[Ga(NH_3)_2F_4]^-$ complex ions may be present. This observation may be the key to the enravelment of solubility and crystallization processes during GaN crystal growth.

#### 4.2.3. Intermediate Species controlling Solubility and Growth Rates

There is little known about the solubility of group III nitrides in supercritical ammonia. We believe it to strongly depend on the present intermediate compounds and thus on mineralizer, temperature and pressure. In the system Ga/$NH_3$ a retrograde solubility for GaN in supercritical ammonia using $KNH_2$ as mineralizer was found, meaning that the solubility of GaN decreases with increasing temperature. This results from experiments, where a Ga nutrient was placed at the midpoint of an autoclave, presenting a temperature gradient with a hot and a cold zone, and observing the crystallization spot are shown. At $T \geq 723$ K, GaN crystallizes in the hot zone [65,67,86]. An equivalent behavior was observed for AlN, which can be formed from Al and $KNH_2$ probably via the intermediate $K[Ga(NH_2)_4]$ [78]. This observation might be attributed to dynamic temperature dependant equilibria of different potassium amides and imides of gallium as intermediate species. $K[Ga(NH_2)_4]$, with tetrahedrally coordinated Ga, is known from synthesis in liquid ammonia [80]. At 853 K and 100 MPa we obtain from Ga and $KNH_2$ pure *h*-GaN. At 733 K and 50 MPa the same starting materials yield a liquid with the composition "$KGa(NH_2)_2(NH)$", which was earlier reported as "$KGa(NH)_n \cdot xNH_3$" [65]. This liquid is supposed to behave similarly to the intermediate "$NaAl(NH_2)_2(NH)$", which occurs during thermal decomposition of $Na[Al(NH_2)_4]$ under release of ammonia (see paragraph *Ammonobasic Systems*) [81]. The coordination of gallium in this liquid is not yet known. Initial results assume a similar behavior for the system Na/Ga/$NH_3$, where the compounds $Na[Ga(NH_2)_4]$ [81] and $Na_2[Ga(NH_2)_4]NH_2$ [67,82] are known and the existence of an equivalent liquid phase is possible.

In ammonoacidic milieu, negative and positive temperature dependance of the solubilities are observed. For the temperature range 473–823 K GaN shows a positive temperature dependance of the solubility in ammonoacidic milieu, using $NH_4X$ ($X$ = Cl, Br, I) as mineralizer [87,88]. This is observed for the syntheses of *c*-GaN and *h*-GaN with Ga metal or GaN as nutrient [88]. Additionally, there are two examples of GaN manifesting a negative solubility in ammonoacidic milieu reported: A change in the temperature dependance of the solubility of GaN from positive to negative, using $NH_4Cl$ has been noticed at temperatures above 923 K with pressures of 110 MPa [62]. Also, a negative solubility has been revealed in the temperature range 823–923 K using $NH_4F$ as mineralizer [46]. Up to now $NH_4F$ and $NH_4Cl$ are the only acidic mineralizers known to evoke a negative solubility for GaN and consequently the crystallization in the hot zone.

Different growth rates for the negatively charged $(000\bar{1})$ *N*-face and the positively charged (0001) Ga-face of the GaN seed crystal were observed. It is assumed that the nature of the intermediate species determines the predominant growth on one of the faces. Thus, the existence of positively charged complex ions such as $[Ga(NH_3)_6]^{3+}$ and $[Ga(NH_3)_5Cl]^{2+}$ may explain a higher growth rate on the negatively charged face (see Figure 6a) [87]. Furthermore, a growth on both *c*-faces, the negatively charged *N*-face and the positively charged Ga-face, is observed using $NH_4F$ as mineralizer [46]. The presence of both cationic $[Ga(NH_3)_4F_2]^+$ and anionic $[Ga(NH_3)_2F_4]^-$ complex ions as intermediates in solution, which should deposit each on the opposite charged face of the GaN seed, may explain this

phenomenon (see Figure 6b). Consequently, the solubility, the crystallization zone and the deposition on the seed crystal of group III nitrides dependent strongly on the formed intermediate compounds.

**Figure 6.** Schematic crystallization of GaN on a seed crystal under ammonoacidic conditions. (**a**) by cationic $[Ga(NH_3)_4F_2]^+$ and anionic $[Ga(NH_3)_2F_4]^-$ intermediates, (using $NH_4F$ as mineralizer), manifesting a negative temperature dependance of the solubility of GaN; (**b**) by cationic $[Ga(NH_3)_6]^{3+}$ intermediates (using $NH_4Br$ or $NH_4I$ as mineralizer), manifesting a positive temperature dependance of the solubility of GaN.

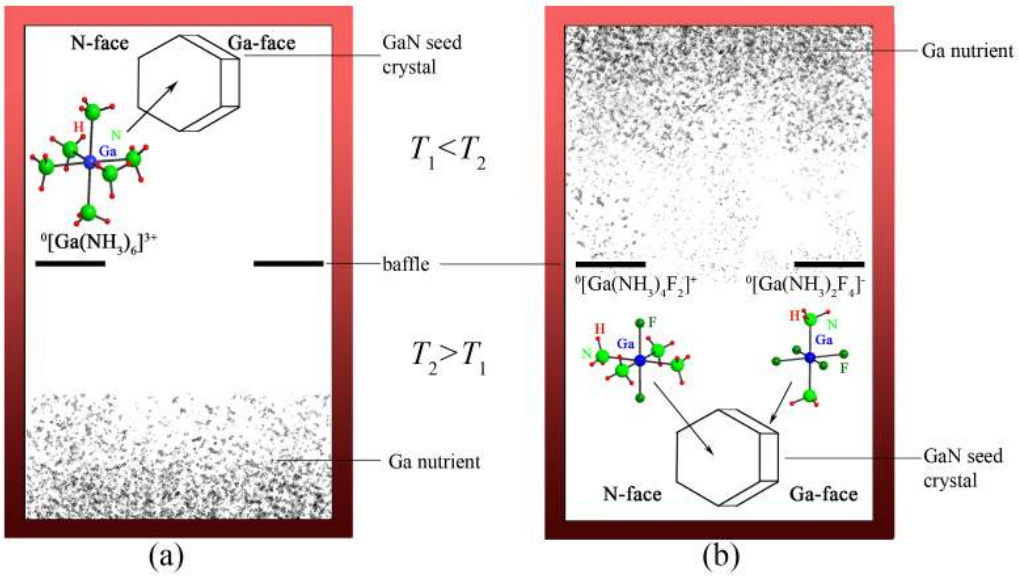


## 5. Compounds from Ammonothermal Synthesis

### *5.1. Ammoniates of Metal Halides*

Ammoniates of metal halides can be grown from metal halides or from the metal and ammonium halides in supercritical ammonia (see Table 3). Such ammoniates of metal halides are suggested to represent crystallized intermediate compounds during ammonoacidic III-nitride growth [66], since ammoniates are expected to have a high solubility in supercritical ammonia (see paragraph *Ammonoacidic Systems*). In liquid and supercritical ammonia, one typically obtains the ammoniates with highest ammonia content known, for example, $[Al(NH_3)_6]I_3 \cdot NH_3$ [89], $[Al(NH_3)_5Cl]Cl_2$, $[Al(NH_3)_5Br]Br_2$, $[Al(NH_3)_5I]I_2$ [84], $[Ga(NH_3)_6]I_3 \cdot NH_3$, $[Ga(NH_3)_6]Br_3 \cdot NH_3$, $[Ga(NH_3)_5Cl]Cl_2$, $Ga(NH_3)_3F_3$ [66], $[Fe(NH_3)_6]I_2$ and $[Mn(NH_3)_6]I_2$ [90].

Other synthesis methods leading to metal ammoniates are reaction of metal halides with gaseous ammonia or reaction of metals with ammonia donors (e.g., $NH_4HF_2$, $NH_4Cl$, $NH_4Br$) producing compounds such as $Mg(NH_3)_2Cl_2$, $Mg(NH_3)_2Br_2$, $Mg(NH_3)_2I_2$ [91], $[Zn(NH_3)_4]Br_2$, $[Zn(NH_3)_4]I_2$ [92], $Ga(NH_3)_2F_3$ [93], $Fe(NH_3)_2Cl_2$, $[Fe(NH_3)_6]Cl_2$, $[Fe(NH_3)_6]Br_2$ [94–96] and $[B(NH_3)_5Cl]Cl_2$ with $B$ = Al [84], Cr [97], Co [97,98], Rh [97,99], Ru [97], Os [97]. Further ammoniates may be obtained by thermal decomposition of higher ammoniates. The step-wise ammonia release on heating

of $[Fe(NH_3)_6]Cl_2$ via $Fe(NH_3)_2Cl_2$ and amorphous $Fe(NH_3)Cl_2$ to $\epsilon$-$Fe_3N_{1+x}$ illustrates the formation of different metal halide ammoniates by thermal decomposition [94–96].

**Table 3.** Conditions for the ammonothermal crystal growth of metal halide ammoniates and of ammoniates of metal amides.

| Compound | Reactants + mineralizer | *T*/K | *p*/MPa | *t*/d | References |
|---|---|---|---|---|---|
| $Al(NH_3)_2F_3$ | $AlN + NH_4F$ | 673 | – | 3 | [83] |
| $[Al(NH_3)_5Cl]Cl_2$ | $AlCl_3$ | 603 | – | 3–6 | [84] |
| $[Al(NH_3)_5Br]Br_2$ | $AlBr_3$ | 623 | – | 3–6 | [84] |
| $[Al(NH_3)_5I]I_2$ | $AlI_3$ | 673 | – | 3–6 | [84] |
| $[Al(NH_3)_6]I_3 \cdot NH_3$ | $Al + NH_4I$ | 393 | 9 | 1 | [89] |
| $Ga(NH_3)_3F_3$ | $Ga + NH_4F$ | 753 | 238 | 3 | [66] |
| $[Ga(NH_3)_5Cl]Cl_2$ | $Ga + NH_4Cl$ | 853 | 95 | 1 | [66] |
| $[Ga(NH_3)_6]Br_3 \cdot NH_3$ | $GaBr_3$ | 197–373 | $\leq$6 | – | [66] |
| $[Ga(NH_3)_6]I_3 \cdot NH_3$ | $GaI_3$ | 197–373 | $\leq$6 | – | [66] |
| $[Mn(NH_3)_6]I_2$ | $Mn + I_2$ | 673–873 | 600 | $\leq$7 | [90] |
| $[Fe(NH_3)_6]I_2$ | $Fe + I_2$ | 673–873 | 600 | $\leq$7 | [90] |
| $Cs_3La(NH_2)_6 \cdot NH_3$ | Cs + La | 490–570 | 400–600 | 31–103 | [100] |
| $Cs_4La(NH_2)_7 \cdot NH_3$ | Cs + La | 490–570 | 400–600 | 31–103 | [100] |
| $BaAl_2(NH_2)_8 \cdot 2\,NH_3$ | $Al + BaAl_2$ | 823 | 245 | 29 | [101] |
| $InF_2(NH_2) \cdot NH_3$ | $InN + NH_4F$ | 673 | 220 | 1 | [83] |

### *5.2. Binary Amides and Deuteroamides*

Several binary amides were obtained from the metals dissolved in liquid ammonia at ambient temperature. In 1891, Joannis had already discovered liquid ammonia as useful solvent to obtain single crystals of metal amides. He obtained colorless $NaNH_2$ crystals from a solution of Na in liquid ammonia [102]. Europium, ytterbium, alkali and alkaline-earth metals dissolve in liquid ammonia at ambient temperature and form intensely blue or bronze colored solutions, if in higher concentration [103]. The solutions are metastable and react to metal amides in form of colorless crystals, hydrogen and a colorless solution [104]. The formation of amides can be enhanced by higher temperatures, higher pressures, exposure to light or addition of a catalyst, e.g., elemental platinum or Fe(II)-compounds like iron oxide [49,73,74,105,106].

#### 5.2.1. Alkali Metal Amides

The alkali metal amides $LiNH_2$ [107], $NaNH_2$ [108], $KNH_2$, $RbNH_2$ and $CsNH_2$ [73] can be obtained from the metals in liquid ammonia at ambient temperature. The presence of a catalyst (platinum net) or exposure to light enhances the reaction rate. The reaction duration depends on the solubility of the metal in liquid ammonia, which rises with increasing atomic weight of the alkali metal. Higher temperatures accelerate the reactions considerably. For $KNH_2$, $RbNH_2$ and $CsNH_2$ the reaction can be carried out within a few hours even at low temperatures ($T \leq 273$ K), usually yielding micro crystalline

powders [106]. The formation of $LiNH_2$ from lithium metal and liquid ammonia at ambient temperature takes 8 days or more [73,107]. At 400 K and 20 MPa the reaction can be carried out within one day without any catalyst [109], after seven days at 583 K and 71 MPa crystals were obtained [1]. $NaNH_2$ shows similar behavior [108]. To shorten the reaction time and to grow alkali metal amide crystals, it is favorable to work under ammonothermal conditions (see Table 4) [1].

**Table 4.** Conditions for the ammonothermal synthesis of binary amides and deuteroamides (synthesized using $ND_3$).

| Compound | Reactants + mineralizer | *T*/K | *p*/MPa | *t*/d | Sample | References |
|---|---|---|---|---|---|---|
| $LiND_2$ | Li | 473 | 304 | – | m.c. | [110] |
| $NaNH_2$ | Na | 393 | ≤10 | 14 | s.c. | [111] |
| $NaND_2$ | Na | 423–473 | 405 | 8 | m.c. | [111] |
| $KND_2$ | K | 320 | ≤10 | 4 | m.c. | [112] |
| $CsNH_2$ | Cs | 423 | 180 | 2 | m.c. | [113] |
| $CsND_2$ | Cs | 423 | 180 | 2 | m.c. | [113] |
| $Be(NH_2)_2$ | Be | 633 | 253 | 5 | s.c. | [2] |
| $Be(NH_2)_2$ | Be + $NaN_3$ | 643 | 355 | 20 | s.c. | [114] |
| $Mg(NH_2)_2$ | Mg | 613–653 | 10 | 2 | m.c. | [115] |
| $Mg(NH_2)_2$ | Mg + $NaN_3$ | 523 | 253 | 2–4 | s.c. | [1,2] |
| $Mg(NH_2)_2$ | $Mg_3N_2$ | 633–648 | 1 | ≤7 | m.c. | [115] |
| $Mg(NH_2)_2$ | Mg + $NaNH_2$ | 623–653 | 212–345 | 2–4 | s.c. | [115] |
| $Ca(NH_2)_2$ | Ca | 370 | 6 | 14 | s.c. | [116] |
| $Sr(NH_2)_2$ | Sr + K | 625 | 550 | 7 | s.c. | [117] |
| $Sr(ND_2)_2$ | Sr | 625 | 550 | 9 | m.c. | [117] |
| $Ba(NH_2)_2$ | Ba | 533 | 324 | 3 | s.c. | [1] |
| $Ba(NH_2)_2$ | Ba | 398 | ≤20 | 120 | s.c. | [118] |
| $Mn(NH_2)_2$ | Mn + $Na_2[Mn(NH_2)_4]$ | 393 | 10 | 10 | s.c. | [119] |
| $Zn(NH_2)_2$ | Zn + $Na_2[Zn(NH_2)_4] \cdot 0 \cdot 5\,NH_3$ | 523 | 380 | 60 | s.c. | [119] |
| $La(NH_2)_3$ | La + $KNH_2$ | 623 | 405 | 6 | s.c. | [120] |
| $Sm(NH_2)_3$ | Sm | 403–493 | 200–500 | – | – | [121] |
| $Eu(NH_2)_2$ | Eu + K | 523–673 | 500–557 | 7–9 | s.c. | [122] |
| $Eu(NH_2)_2$ | Eu | 323 | ≥0.9 | 3 | m.c. | [123] |
| $Yb(NH_2)_3$ | Yb | 453 | 507 | 32 | m.c. | [123] |

s.c. means single crystal, m.c. micro crystalline.

Although crystals of the heavier alkali metal amides were obtained from liquid ammonia, the atomic positions of hydrogen could not be determined with X-ray diffraction. This stems back to the low scattering contribution of hydrogen in combination with these metals. Neutron diffraction of the corresponding deuteroamides allows determination of the atomic position for hydrogen. Under ammonothermal conditions, deuteroamides can be grown with small amounts of expensive $ND_3$, while getting fast a comparatively large yield per synthesis. The exact atomic position provided the base for the interpretation of the interesting electrostatic interactions between the protons and the cations, due

to an asymmetric distribution of the charge on $NH_2^-$ [110,111,117,124,125]. An increasing interaction with rising charge density of the cation was observed, *i.e.*, for the amides of the lighter alkali and alkaline-earth metals (Li, Na, Be, Mg) those interactions are stronger than for the heavier ones. In the amides of Li, Na, Be and Mg, the anions form the motif of a cubic closed packing with the cations occupying tetrahedral holes. The resulting structures show an occupation of specific tetrahedral holes within the anion substructure by the cations and can even lead to layered structures similar to LiOH [126]. In lithium amide, Li occupies alternatingly 3/4 of the tetrahedral holes within one layer and 1/4 within the next. Due to strong proton–cation interactions, the anion is hindered in vibration. For the heavier metals the coordination number increases to six for K, Rb, Ca and Sr and eight for Cs. The interatomic interactions decrease resulting in the realization of several modifications, depending on the vibrational and rotational freedom of the amide ions influenced by temperature, as can be seen in the case of $KNH_2$ [3,124,125,127,128].

Alkali metal amides are important starting materials in ammonothermal synthesis, due to their application as ammonobasic mineralizers. $NaNH_2$ and $KNH_2$ are the most used ones, since they are less reactive than $RbNH_2$ and $CsNH_2$, but show a higher solubility as $LiNH_2$. The solubility of alkali metal amides in liquid ammonia increases with increasing atomic weight. $LiNH_2$ is only very poorly soluble in liquid ammonia, $NaNH_2$ is poorly soluble (0.144 g/100 g $NH_3$ at 253 K), $KNH_2$ is well soluble (65.8 g/100 g $NH_3$ at 241 K), $RbNH_2$ is very soluble (several hundred grams/100 g $NH_3$ at 241 K) and $CsNH_2$ is little less soluble as $RbNH_2$ [73,129].

#### 5.2.2. Alkaline-Earth Metal Amides

The alkaline-earth metal amides $Mg(NH_2)_2$, $Ca(NH_2)_2$, $Sr(NH_2)_2$ and $Ba(NH_2)_2$ are obtained from the metals in liquid ammonia at ambient temperature with reaction times of two days ($Ba(NH_2)_2$), eight days ($Sr(NH_2)_2$), four months ($Ca(NH_2)_2$) [130] and up to 1.5–2 years ($Mg(NH_2)_2$) [115]. $Mg(NH_2)_2$ and $Ba(NH_2)_2$ crystals, produced in this way, were not suitable for X-ray diffraction and no $Be(NH_2)_2$ could be obtained. For the heavier alkaline-earth metals (Ca, Sr, Ba) temperatures and pressures somewhat below the critical point of ammonia are sufficient to obtain well crystallized amides and deuteroamides. For the synthesis of $Ca(NH_2)_2$, $Ca(ND_2)_2$, $Sr(NH_2)_2$ and $Sr(ND_2)_2$ 370 K and 6 MPa were applied for two weeks starting from the metal and ammonia [116], $Ba(NH_2)_2$ crystals were obtained at 398 K and $\leq$20 MPa after four months [118]. Nevertheless, working under ammonothermal conditions reduces the reaction time considerably and micro crystalline $Ba(NH_2)_2$ and $Sr(NH_2)_2$ can be obtained from the respective metals in supercritical ammonia after 2 days at 573 K and 60 MPa. Increasing the reaction conditions for $Mg(NH_2)_2$ from $\sim$0.09 MPa and ambient temperature to $\sim$10 MPa and 613–653 K reduces the reaction time from 1.5–2 years to two days and forms a micro crystalline product suitable for powder X-ray diffraction [115]. $Mg(NH_2)_2$ crystals were obtained from Mg metal under ammonobasic conditions (using $NaNH_2$ or $NaN_3$ as mineralizers) at 523–653 K and 10–345 MPa [1,2,115]. The reaction of $Mg_3N_2$ at elevated temperatures of 633–648 K and $NH_3$ pressure of 1 MPa also yields micro crystalline $Mg(NH_2)_2$ [115]. First synthesis of $Be(NH_2)_2$ proceeded under ammonothermal conditions: Single crystals were obtained from the reaction of beryllium metal and ammonia with $NaN_3$ as mineralizer at 643 K and 355 MPa after 20 days [114].

### 5.2.3. Lanthanum Amide, Samarium Amide, Europium Amide and Ytterbium Amide

Apart from $Yb(NH_2)_3$ [123] and $Sm(NH_2)_3$ [121], $La(NH_2)_3$ [120] is the only binary trivalent rare-earth metal amide so far. Colorless single crystals are obtained from the reaction of lanthanum metal and potassium (molar ratio 80:1) in supercritical ammonia at 623 K and 405 MPa after six days. The use of a mineralizer is crucial for the crystal growth, without only micro crystalline powder is produced. Using $NH_4I$ as mineralizers leads to smaller crystals than presented for the reaction in presence of the potassium mineralizer [120,131]. $Sm(NH_2)_3$ was obtained from samarium metal and potassium (molar ratio 23:1) in supercritical ammonia at 403–493 K and 200–500 MPa as micro crystalline powder [121]. A solution of europium in liquid ammonia already forms micro crystalline $Eu^{II}(NH_2)_2$ at 323 K and $\geq$0.9 MPa. Increasing the temperature and pressure to 523–673 K and 500–557 MPa and using optionally potassium as mineralizer leads to dark red crystals. The amount of mineralizer is crucial for the formation of the binary amide, since two ternary amides, namely $K[Eu^{II}(NH_2)_3]$ and $K_3[Eu^{III}(NH_2)_6]$, can be obtained in the same temperature and pressure range [122,123]. There are two binary ytterbium amides known, $Yb(NH_2)_2$ and $Yb(NH_2)_3$, which were so far only obtained as micro crystalline powders. $Yb(NH_2)_2$ was prepared from ytterbium metal in liquid ammonia at ambient temperature within some hours and forms with ammonia $Yb(NH_2)_3$, already before all metal has reacted to $Yb(NH_2)_2$ [123]. Nearly pure $Yb(NH_2)_3$ was obtained from ammonothermal conditions (453 K, 507 MPa, 32 days), however, no successful crystal structure determination for $Yb(NH_2)_3$ was presented so far [123].

### 5.2.4. Transition Metal, Group III and Group IV Metal Amides

There are various synthetic methods leading to binary transition metal amides. Some transition metal amides precipitate from metal salt solutions in liquid ammonia in presence of $KNH_2$, e.g., $Cd(NH_2)_2$ can be obtained from $Cd(SCN)_2$ [74,132]. Earlier, binary metal amides were obtained from the reaction from the metal with gaseous or liquid ammonia or of a metal ethyl compound with ammonia, e.g., $Zn(NH_2)_2$ [133]. As a result of these synthesis techniques conducted at comparably low temperatures, the products are often amorphous or poorly crystallized. Under ammonothermal conditions, such poorly crystallized or amorphous binary amides can be recrystallized in form of single crystals or well crystallized powders. Alternatively, they yield from the metal in presence of a mineralizer under ammonothermal conditions: Amorphous zinc amide can be recrystallized at 723 K and 30.4 MPa [1]. Zinc amide was first crystallized under ammonothermal conditions, subsequently the crystal structure was determined. Crystals were obtained from zinc powder and ammonia with $Na_2[Zn(NH_2)_4]\cdot 0.5\ NH_3$ as mineralizer at 523 K and 380 MPa [119]. The analogous reaction of Mn and ammonia at 393 K and 10 MPa (slightly lower than the critical pressure) using $Na_2[Mn(NH_2)_4]$ as mineralizer yielded $Mn(NH_2)_2$ [119].

Binary group III amides are potential precursors during ammonothermal synthesis of group III nitrides. However, the correctness of the reported formula $B(NH_2)_3$ ($B$ = B, Al, Ga, In) was questioned or could not be reproduced. The lack of crystal structure data for these compounds hinders an unequivocal chemical assignment. $B(NH_2)_3$ obtained from $BCl_3$ or $BBr_3$ with $NH_4Cl$ in liquid ammonia [134] is suspected to represent polymeric $B(NH)_{3/2}$ (see paragraph *Imides, Nitride Imides, Nitride Amides and*

*Amide Azides*) [135]. The reaction of $AlBr_3$ and $KNH_2$ in liquid ammonia did not yield $Al(NH_2)_3$, but a mixed polymeric aluminum amide imide $[Al(NH_2)(NH)]_n$ (see paragraph *Imides, Nitride Imides, Nitride Amides and Amide Azides*) [135–137]. The reaction of $A(1)[Ga(NH_2)_4]$ with $NH_4Cl$ in liquid ammonia at 237 K yields an amorphous product, with the proposed formula $Ga(NH_2)_3$. Due to the lack of diffraction data no crystal structures are proposed, although the composition was determined by chemical analysis [80]. Polymeric gallium imide $[Ga(NH_{3/2}]_n$ was reported from the reaction of $[Ga(NMe_2)_3]_2$ with liquid ammonia in reflux for 8 h (see paragraph *Imides, Nitride Imides, Nitride Amides and Amide Azides*) [135].

$In(NH_2)_3$ crystals were obtained from $KNH_2$ and $InI_3$ or $K_3In(NH_2)_6$ in liquid ammonia after one day. Several ternary alkali metal indium amides are known from snythesis in liquid ammonia, e.g., $Li_3In(NH_2)_6$, $K_2In(NH_2)_5$, $K_3In(NH_2)_6$ [138]. However, since no structural information on these compounds is available, the compositions might be questioned.

$Si(NH_2)_4$ is obtained from $SiCl_4$ in liquid ammonia at $T \leq 273$ K and decomposes at $T \geq 373$ K to $Si(NH)_2$ [139,140]. Again, no crystal structure data for $Si(NH_2)_4$ and $Si(NH)_2$ are reported due to the lack of crystalline products. The chemical nature of the compounds for now remains to be proven.

### *5.3. Ternary Amides*

There were various ternary amides of the formulas $A(1)^I_nA(1)^I_m(NH_2)_{n+m}$, $A(1)^I_nA(2)^{II}_m/M^{II}_m/R^{II}_m(NH_2)_{n+2\cdot m}$, $A(1)^I_nB^{III}/R^{III}(NH_2)_{n+3}$ ($A(1)$ = alkali metal, $A(2)$ = alkaline-earth metal, $M$ = transition metal, $R$ = rare-eart metal, $B$ = main group metal; $n$ = 1, 2, 3; $m$ = 1, 3, 7) obtained from liquid or supercritical ammonia. Usually, they contain two different metals, from which at least one is an alkali or alkaline-earth metal. Examples for ternary amides were reported from syntheses in liquid ammonia, e.g., $A(1)[Al(NH_2)_4]$ (with $A(1)$ = Na, K, Cs) [81,141], $Na_2Al(NH_2)_5$ [82], $Na[Ga(NH_2)_4]$ [81], $KBe(NH_2)_3$ [142], $RbBe(NH_2)_3$ [142], $Li[Al(NH_2)_4]$ [143], α-$K[Al(NH_2)_4]$ and β-$K[Al(NH_2)_4]$ [144]. By increasing temperature and pressure the list of ternary amides was extended and the structure determination often was possible (see Tables 5–7), since crystal growth was realized only under ammonothermal conditions, e.g., for $Na_2[Ga(NH_2)_4]NH_2$ [67,82]. Such compounds are expected to exhibit significantly higher solubilities in supercritical $NH_3$. Therefore, they are suggested as intermediates formed from the reactant and the mineralizer during nitride crystal growth of, for example, GaN. The isolation and crystallization of such compounds sheds light on the formation mechanism of the nitride crystal growth.

For the preparation of ternary alkali and alkaline-earth metal amides some tendencies has been established, which can often also be applied to other ternary amides. Thus, it is recommendable to use a surplus of the less soluble metal. In general, alkali metals possess a higher solubility in ammonia than alkaline-earth metals. The same applies for amides of the heavier metals compared to their lighter homologues. The thermal stability of ternary amides decreases with increasing charge density of the cations. At higher temperatures nitrides of the $A(2)$, $M$, $R$ or $B$ metal and binary amides of the alkali metals are formed. The water and oxygen sensitivity of the ternary amides increases with increasing atomic weight of the metal. In the case of ternary alkali metal alkaline-earth metal amides they depend more of the alkali metal than of the alkaline-earth metal [3].

**Table 5.** Conditions for the ammonothermal synthesis of alkali metal alkaline-earth metal ternary amides and coordination numbers of the metal atoms by amide ions.

| Compound | *CN A*(1), *A*(1)/*A*(2) by $NH_2^-$ | Reactants | *T*/K | *p*/MPa | *t*/d | References |
|---|---|---|---|---|---|---|
| $K_2Li(NH_2)_3$ | 6, 4 | K + Li 2:1 | 333 | 70 | 60 | [145,146] |
| $KLi(NH_2)_2$ | [a], 4 | K + Li 1:1 | 333–473 | 70–210 | 4 | [145] |
| $KLi_3(NH_2)_4$ | 8, 4 | K ≤ Li | 333–473 | 70–210 | 4 | [145] |
| $KLi_7(NH_2)_8$ | 8, 4 | K ≤ Li | 333–473 | 70–210 | 4 | [145] |
| $K_2[Mg(NH_2)_4]$ | 7, 4 | K + Mg | 423 | 200 | 3 | [147] |
| $Rb_2[Mg(NH_2)_4]$ | 7, 4 | Rb + Mg | 423 | 200 | 3 | [147] |
| $Cs[Mg(NH_2)_4]$ | 9/11, 4 | Cs + Mg | 415 | 200 | 2 | [148] |
| $NaCa(NH_2)_3$ | 6, 6 | Na + Ca 5:1–1:2 | 740–773 | 500 | 60 | [149,150] |
| $KCa(NH_2)_3$ | 6, 6 | K + Ca 1:1 | 573 | 500 | 20 | [151] |
| $RbCa(NH_2)_3$ | 8, 6 | Rb + Ca 1:2–3:1 | 573 | 500 | 17 | [152] |
| $CsCa(NH_2)_3$ | 8, 6 | Cs + Ca | 573–773 | 500–600 | 10–35 | [153] |
| $KSr(NH_2)_3$ | 6, 6 | K + Sr 1:1 | 570 | 500 | 7 | [149] |
| $RbSr(NH_2)_3$ | 6, 6 | Rb + Sr 3:1–1:1 | 540–573 | 800 | 8 | [150] |
| $CsSr(NH_2)_3$ | 8, 6 | Cs + Sr | 573–673 | 500–600 | 14–55 | [153] |
| $KBa(NH_2)_3$ | 6, 6 | K + Ba 3:1–1:1 | 540–573 | 500 | 7 | [150] |
| $RbBa(NH_2)_3$ | 6, 6 | Rb + Ba 3:1–1:1 | 540–573 | 500 | 7 | [150] |
| $CsBa(NH_2)_3$ | 8, 6 | Cs + Ba | 473 | 500 | 11 | [154] |
| $Na_2Sr_3(NH_2)_8$ | 6, 6 | Na + Sr 1:2 | 570 | 500 | 4 | [149] |

[a] Coordination number uncertain cf. [3].

**Table 6.** Conditions for the ammonothermal synthesis of ternary amides containing rare-earth metals and coordination numbers of the metal atoms by amide ions.

| Compound | *CN A*(1), *R* by $NH_2^-$ | Reactants | *T*/K | *p*/MPa | *t*/d | References |
|---|---|---|---|---|---|---|
| $Na_3[La(NH_2)_6]$ | 6, 6 | Na + La 1:1 | 523 | 507 | 30 | [131] |
| $KLa_2(NH_2)_7$ | 6, 8 | K + La 1:2 | 623 | 507 | 6 | [155] |
| $K_3[La(NH_2)_6]$ | 6, 6 | K + La | 473 | 405 | – | [156] |
| $RbLa_2(NH_2)_7$ | [a] | | | | | [3] |
| $Rb_3[La(NH_2)_6]$ | 6, 6 | Rb + La 3:1 | 573 | 400–450 | 6–12 | [157] |
| $CsLa_2(NH_2)_7$ | 9, 8 | Cs + La | 470–570 | 400–600 | 3–100 | [3,158] |
| $Na_3[Ce(NH_2)_6]$ | [a] | | | | | [3] |
| $KCe_2(NH_2)_7$ | 6, 8 | K + Ce 1:1 | 455 | 400–500 | 5–10 | [76] |
| $K_3[Ce(NH_2)_6]$ | 6, 6 | K + Ce 3:1 | 455 | 400–500 | 5–10 | [76] |
| $Cs_3Ce_2(NH_2)_9$ | 12, 6 | Cs + Ce | 490 | 600 | 21 | [159] |
| $Cs_3Ce_2(NH_2)_9$ | 12, 6 | Cs + Ce | 490 | 200 | 21 | [159] |
| $Na_3[Nd(NH_2)_6]$ | 6, 6 | [a] | | | | [3] |
| $KNd_2(NH_2)_7$ | 6, 8 | [a] | | | | [3] |

**Table 6.** *Cont.*

| Compound | *CN A*(1), *R* by $NH_2^-$ | Reactants | *T*/K | *p*/MPa | *t*/d | References |
|---|---|---|---|---|---|---|
| $K_3[Nd(NH_2)_6]$ | 6, 6 | [a] | | | | [3] |
| $Rb_3[Nd(NH_2)_6]$ | 6, 6 | Rb + Nd 3:1 | 573 | 400 | 7 | [157] |
| $Cs_3Nd_2(NH_2)_9]$ | 12, 6 | Cs + Nd | 430–530 | 300 | 7–100 | [159] |
| $Na_3[Sm(NH_2)_6]$ | 6, 6 | [a] | | | | [3] |
| $KSm_2(NH_2)_7$ | 6, 8 | K + Sm 1:2 | 403–493 | 200–500 | – | [121] |
| $K_3[Sm(NH_2)]_6$ | 6, 6 | K + Sm 3:1 | 403–493 | 200–500 | – | [121] |
| $Cs_3Sm_2(NH_2)_9$ | 12, 6 | Cs + Sm | 470 | 600 | 60 | [159] |
| $KEu(NH_2)_3$ | 6, 6 | K + Eu 1:1 | 573 | 500 | 3 | [122] |
| $RbEu(NH_2)_3$ | 6, 6 | Rb + Eu 1:1-2:1 | 540–73 | 500 | 28 | [150] |
| $Rb_3[Eu(NH_2)_6]$ | 10, 6 | Rb + Eu 10:1 | 423 | 500 | 40 | [160] |
| $CsEu(NH_2)_3$ | 6, 6 | Cs + Eu | 573 | 500–600 | 9–14 | [153] |
| $K_3[Eu(NH_2)_6]$ | 6, 6 | K + Eu 12:1 | 573 | 500 | 3 | [122,149] |
| $Na_2Eu_3(NH_2)_8$ | 6, 6 | Na + Eu 1:1 | 570 | 500 | 8 | [149] |
| $NaGd(NH_2)_4$ | 4, 6 | $NaNH_2$ + Gd 1:1 | 493 | 507 | 20 | [161] |
| $Na_3[Gd(NH_2)_6]$ | 6, 6 | $NaNH_2$ + Gd 3:1 | 573 | 304 | 51 | [3,161] |
| $K_3[Gd(NH_2)_6]$ | 6, 6 | [a] | | | | [3] |
| $Cs_3Gd_2(NH_2)_9$ | 12, 6 | Cs + Gd | 440 | 600 | 160 | [162] |
| $NaY(NH_2)_4$ | 6, 6 | Na + Y 1:1 | 523 | 507 | 7 | [163] |
| $KY(NH_2)_4$ | 6, 6 | K + Y 1:4–6 | 485–505 | 600 | 22 | [164] |
| $RbY(NH_2)_4$ | 11, 6 | Rb + Y 1:4–6 | 485–505 | 600 | 22 | [164] |
| $Na_3[Y(NH_2)_6]$ | 6, 6 | Na + Y 3:1 | 523 | 507 | 7 | [163] |
| $Cs_3Y_2(NH_2)_9$ | 12, 6 | Cs + Y | 490 | 600 | 70 | [162] |
| $Rb_3[Y(NH_2)_6]$ | 10, 6 | Rb + Y 3:1 | 473 | 500 | 14 | [157,160] |
| $K_3[Y(NH_2)_6]$ | 10, 6 | K + Y 3:1 | 473 | 500 | 14 | [157,160] |
| $NaYb(NH_2)_4$ | 4, 6 | Na + Yb 1:1 | 413–463 | 507 | 14 | [163] |
| $Na_3[Yb(NH_2)_6]$ | 6, 6 | Na + Yb 3:1 | 453 | 608 | 8 | [165] |
| $KYb(NH_2)_7$ | [a] | | | | | [3,121] |
| $K_3[Yb(NH_2)_6]$ | 10, 6 | K + Yb 3:1 | 473 | 500 | 14 | [157,160] |
| $Rb_3[Yb(NH_2)_6]$ | 8, 6 | Rb + Yb 3:1 | 473 | 500 | 14 | [157,160] |
| $Cs_3Yb_2(NH_2)_9$ | 12, 6 | Cs + Yb | 450 | 600 | 160 | [162] |

[a] No further information in literature.

**Table 7.** Conditions for the ammonothermal synthesis of ternary amides of main group and transition metals and coordination numbers of the metal atoms by amide ions.

| Compound | *CN A*(1), *B*/*M* by $NH_2^-$ | Reactants | *T*/K | *p*/MPa | *t*/d | References |
|---|---|---|---|---|---|---|
| $Li[Ga(NH_2)_4]$ | 4, 4 | Ga + $LiNH_2$ | 673 | 250 | 3 | [67] |
| $Li[Ga(NH_2)_4]$ | 4, 4 | Ga + $LiNH_2$ | 673 | 250 | 3 | [67] |
| $Na_2[Ga(NH_2)_4]NH_2$ | 4, 4 | Ga + $NaNH_2$ | 853 | 130 | 2 | [67,82] |
| $Na[Ga(NH_2)_4]$ | 4, 4 | Na + Ga | 853 | 130 | 2 | [67,81] |
| $Rb[Al(NH_2)_4]$ | 12, 4 | Rb + Al | 393–473 | 80–120 | 20 | [166] |
| $Cs[Al(NH_2)_4]$ | 12, 4 | Cs + Al | 423–473 | 120–600 | 15 | [166] |
| $Na_2[Mn(NH_2)_4]$ | 4/6, 4 | Na + Mn | 373 | 10 | – | [167] |
| $K_2[Zn(NH_2)_4]$ | 7, 4 | Zn + $KNH_2$ | 720 | 249 | 2 | [168] |

Both the nature of the $A(1)$ and the $A(2)$, $M$, $R$ or $B$ metal have an impact on the crystal structure, the number of compounds formed and the composition of the ternary amide. The charge density of both cations is crucial for the realized structure. Increasing the size of the alkali metal leads in the case of ternary lanthanum amides to different structures for $Na_3[La(NH_2)_6]$ [131], $K_3[La(NH_2)_6]$ [156] and $Rb_3[La(NH_2)_6]$ [157]: In $Na_3[La(NH_2)_6]$ all cations occupy octahedral sites in a close packing of amide ions with ABC stacking. In $K_3[La(NH_2)_6]$ both types of cations occupy octahedral sites in a close packing of amide ions with ABC stacking, one layer of octahedral voids is fully occupied by K cations, in the next layer one third of the octahedral voids is filled with La atoms. For $K_3[R(NH_2)_6]$ ($R$ = Y, La, Ce, Nd, Sm, Eu, Gd, Yb) two structure types were observed, one for rare-earth metals from La to Gd and one for Y and Yb. The first group crystallizes in $C2/m$ with all cations in octahedral holes of a close packing of amide groups, occupying layers of octahedral holes alternately. The second group consists of $K_3[Y(NH_2)_6]$ and $K_3[Yb(NH_2)_6]$, which are isotypes of $Rb_3[Eu(NH_2)_6]$ and $Rb_3[Y(NH_2)_6]$ [160]. Those compounds crystallize in $R32$. $R^{3+}$ cations occupy octahedral holes in a close packing of amide groups, while $A^+$ cations are surrounded by a larger number of amide groups. In $Rb_3[La(NH_2)_6]$ [157] again the cations are surrounded octahedrally, realizing layers. Perhaps surprisingly, there is no such compound as $Cs_3[La(NH_2)_6]$ known, but two amide ammoniates $Cs_3La(NH_2)_6 \cdot NH_3$ and $Cs_4La(NH_2)_7 \cdot NH_3$ [100], where cesium and amide ions together with ammonia molecules form the motif of a cubic close packing with lanthanum cations in octahedral voids, exclusively formed by amide groups. A change of the structure for compounds of the same composition can be observed with changing charge density of both cation types, as can be seen from alkali metal rare-earth metal amides. Thus, compounds with small charge density realize close packings of amide ions with all cations situated in octahedral holes. With increasing size of the alkali metal, layered structures of the cations are preferred and the rare-earth cations form structural units with the amide groups similar to the binary amides. In the cesium amides cesium is surrounded by twelve amide ions, the $R^{3+}$ ions occupy also octahedral sites in a close packing. $A(1)$-rich phases manifest lower coordination numbers at $A(2)$, $M$, $R$ or $B$ metal, as can be seen in $K_3[La(NH_2)_6]$ [156] and $KLa_2(NH_2)_7$ with $CN$(La) of 8 and 6 respectively [155]. In Table 5 the coordination numbers of the cations by amide ions in ternary alkali metal alkaline-earth metal amides are listed and the change of the surrounding depending on the size of the metals can be compared.

Four different types of ternary alkali metal amides can be distinguished according to their crystal structures: The first group consists of the isotypic compounds $NaCa(NH_2)_3$ [149,150], $KSr(NH_2)_3$ [149], $KBa(NH_2)_3$ [150], $RbBa(NH_2)_3$ [150], $KEu(NH_2)_3$ [122], $RbEu(NH_2)_3$ [150] and $NaY(NH_2)_4$ [163]. The amide groups arrange in the motif of a cubic closed packing, the cations occupy octahedral holes. $Na_2Sr_3(NH_2)_8$ [149], $Na_2Eu_3(NH_2)_8$ [149], $Na_3La(NH_2)_6$ [131] and $Na_3Y(NH_2)_6$ [163] crystallize in the same structure, irrespective of the different composition. This is possible, since in $Na_3R(NH_2)_6$ with $R$ = La, Ce, Nd, Sm, Gd, Y the sites are occupied completely and ordered, whereas for all other compounds a statistical occupation of the sites with different cations is observed [148,150]. Compared to the ternary amides of the smaller alkaline-earth metals, those compounds are more ionic.

In the second group the difference of the radii of the two types of cations is larger, which results in different coordination numbers. Those ternary amides crystallize in the space groups $C2/c$ ($RbCa(NH_2)_3$ [152]) and $P2_1/c$ ($KCa(NH_2)_3$ [151]). Both structures are related by a close structural relationship, since $P2_1/c$ is a translationengleiche maximal subgroup of $C2/c$. The change of the space

group is a result of the influence of the radii of the alkali metals. For potassium a distorted octahedral surrounding is realized, however rubidium and cesium require higher coordination numbers. This group also contains the compounds $CsCa(NH_2)_3$, $CsSr(NH_2)_3$ and $CsEu(NH_2)_3$ [153]. The resulting crystal structures are described as distorted hexagonal perovskites, where cesium and $NH_2^-$ form the motif of a hexagonal close packing. Ca occupies face-sharing octahedral voids exclusively surrounded by amide ions. In this way, one-dimensional chains of $^1_\infty[Ca(NH_2)_6^{4-}]$ result [153]. The change from group one to group two may surprise: One could expect the same crystal structure for $KCa(NH_2)_3$ and $KEu(NH_2)_3$, because the binary amides $Ca(NH_2)_2$ and $Eu(NH_2)_2$ are isotypes [149].

The third group includes $K[Be(NH_2)_3]$ and $Rb[Be(NH_2)_3]$, where nearly trigonal planar complex anions $[Be(NH_2)_3]^-$ appear. Up to now, no amide of this group was obtained from ammonothermal conditions [142].

Finally, the fourth group contains isolated tetrahedral complex anions of the type $[B(NH_2)_4]^{2-}$. Examples, obtained from supercritical ammonia are one modification of dimorphic $K_2[Zn(NH_2)_4]$ [168,169] and $CsMg(NH_2)_4$ [148]. The divalent cation is surrounded by four amide groups, whereas the monovalent cations show coordination with larger numbers of amide groups. Various ternary amides of this type containing two metals were synthesized from liquid ammonia, e.g., $Na_2[Mn(NH_2)_4]$ [169], $Li[Al(NH_2)_4]$ [143,170], $Na[Al(NH_2)_4]$ [81], $Na[Ga(NH_2)_4]$ [81,141], $K_2[Mn(NH_2)_4]$ [171] and $Rb_2[Zn(NH_2)_4]$ [171].

There was a remarkable change of the valence state of Eu from +2 to +3 observed, when a large surplus of $KNH_2$ was used in ammonothermal synthesis of ternary amides. Apparently, an increased $NH_2^-$ concentration provokes formation of $K_3[Eu^{III}(NH_2)_6]$ rather than $KEu^{II}(NH_2)_3$ [122]. Divalent europium is known to behave similarly to divalent strontium and thus it is not surprising that $KEu^{II}(NH_2)_3$ is an isotype of $KSr^{II}(NH_2)_3$ [149]. Trivalent europium behaves rather similar to the trivalent lanthanides: $K_3[Eu^{III}(NH_2)_6]$ is an isotype of $K_3[La^{III}(NH_2)_6]$ [156]. The same applies for the respective ternary rubidium europium amide. Due to the lower solubility of $NaNH_2$ and the resulting lower $NH_2^-$ concentration in this system a product with lower sodium content $Na_2Eu^{II}_3(NH_2)_8$ was obtained in this system [149].

### *5.4. Imides, Nitride Imides, Nitride Amides and Amide Azides*

Certain imides and nitrides can be formed via thermal decomposition of amides under release of ammonia. From *in-situ* powder X-ray diffraction it is known that during decomposition compounds containing $N^{3-}$, $NH_2^-$ and $NH^{2-}$ ions may occur. Examples are $Li_2NH$, CaNH, MgNH [73,114] and $Th_2N_2(NH)$ [33]. There are binary imides of lithium, beryllium, magnesium, calcium, strontium and barium known [73,114]. A few imides and nitride imides were obtained from ammonothermal conditions, but only in the form of micro crystalline powders, see Table 8. From the thermal degradation of ternary rare-earth metal amides the formation of $Yb_{0.66}(NH)$ [123], $Ce_3(NH)_3N$ [76] and $La_{0.667}NH$ [172] was reported.

**Table 8.** Conditions for the ammonothermal synthesis of micro crystalline binary imides, nitride imides and amide azides.

| Compound | Reactants mineralizer | *T*/K | *p*/MPa | *t*/d | References |
|---|---|---|---|---|---|
| MgNH | $Mg_3N_2$ | 773 | ≥5 | 7 | [115] |
| $Th(NH)_2$ | Th + Li/Na/K | 573 | 608 | 29 | [33] |
| $Th_2N_2NH$ | Th | 823 | 507 | 2 | [1] |
| $ThN(NH_2)$ | ThNJ + $A(1)NH_2$ | 573 | 405 | 2 | [33] |
| $Th_3N_2(NH)_3$ | ThNJ + $A(1)NH_2$ | 623 | 608 | 27 | [33] |
| $Si_2N_2NH$ | Si + $KNH_2$ | 873 | 600 | 5 | [173] |
| $ZrN(NH_2)$ | ZrNI + $KN_3$ | 633 | 507 | 10 | [75] |
| $Cs_2(NH_2)N_3$ | Cs + Y | 463–493 | 500–600 | 21–26 | [174] |

The reaction of $Mg_3N_2$ with $NH_3$ at $T \geq 773$ K and $p \geq 5$ MPa yields MgNH with $Mg(NH_2)_2$ and $Mg_3N_2$ impurities after one week. This finding may be explained by the following equations [115]:

$$Mg_3N_2 + NH_3 \rightleftarrows 3MgNH \tag{8}$$

$$MgNH + NH_3 \rightleftarrows Mg(NH_2)_2 \tag{9}$$

MgNH can also be obtained by thermal decomposition of $Mg(NH_2)_2$ at 513–638 K. At 633 K a micro crystalline powder suitable for X-ray diffraction is produced [115]. $Th(NH)_2$ is formed from thorium metal and ammonia at 613 K and 304 MPa after 4 days as micro crystalline powder [1]. At higher temperatures of 823 K and 507 MPa a micro crystalline nitride imide with the composition $Th_2N_2NH$ is formed [1].

A cesium amide azide $Cs_2(NH_2)N_3$ is reported from the reaction of Cs and ammonia in presence of Y at 463–493 K and 500–600 MPa. The appearance of azide ions may be regarded somewhat surprising under the applied conditions, as the nitrogen of the ammonia would become oxidized during formation. Jacobs et al. explained this effect by a drastically reduced volume of the obtained $Cs_2(NH_2)N_3$ compared to the volume of $CsNH_2$ and $NH_3$, assuming release of hydrogen by diffusion through the autoclave wall and perhaps also by formation of yttrium hydride. Following reaction Equation (10) a volume reduction of ∼29% occurs when $Cs_2(NH_2)N_3$ is formed. In addition, the formation of the mixed amide azide in contrast to two compounds ($Cs(NH_2)$ + $CsN_3$) is favorable due to a smaller volume of ∼3% [174].

$$2\,CsNH_2 + 2\,NH_3 \rightleftarrows Cs_2(NH_2)N_3 + 4\,H_2 \tag{10}$$

However, in the past several cyanamides (or carbodiimides, respectively), formed by reaction with unintenional carbon impurities, were initially misinterpreted as representing azide compounds [175,176]. Since any carbon impurity under ammonothermal conditions in presence of alkali or alkaline-earth metals will readily form cyanamide ions [177], it may be regarded as likely that this compound rather represents an amide carbodiimide.

Group III metals manifest a strong tendency to form polymeric imides from synthesis in liquid ammonia. Thus, the reaction of $BX_3$ ($X$ = Cl, Br) and $NH_4Cl$ in liquid ammonia yields a polymeric

solid with the approximate formula $[B(NH)_{3/2}]_n$ [135]. Earlier, a boron amide $B(NH_2)_3$ was discussed to form under similar reaction conditions [134], but this material might be identical to the polymeric $[B(NH)_{3/2}]_n$. In a further report boron imide was obtained from thermal decomposition of $B_2S_3 \cdot 6\,NH_3$ at $T \geq 378$ K [178]. A mixed aluminum amide imide $AlNH_2(NH)$ was reported as intermediate species during AlN synthesis from aluminum hydride $AlH_3$ and liquid ammonia at $T \leq 273$ K. However, the formula was only determined by chemical analysis and no crystal structure determination was reported. A pure aluminum amide $Al(NH_2)_3$ is reported to occur at lower temperatures ($T \leq 223$ K) from the same starting materials and to decompose to AlN via $AlNH_2(NH)$ at $T \geq 243$ K [137]. The metathesis reaction of $AlBr_3$ with $KNH_2$ in liquid ammonia and the reaction of $H_3Al \cdot NMe_3$ with liquid ammonia at ambient temperature yields polymeric $[AlNH_2(NH)]_n$ [135,136]. It is very likely that the reported $AlNH_2(NH)$ is the same polymeric compound [135]. Synthesis of polymeric gallium imide $[Ga(NH_{3/2}]_n$ was reported from the reaction of $[Ga(NMe_2)_3]_2$ with liquid ammonia in reflux for 8 h, the composition was deduced from elemental anaylsis and IR spectroscopy. Thermal decomposition of $[Ga(NH_{3/2}]_n$ yields a mixture of nanosized *c*-GaN and *h*-GaN [135]. Reaction of silicon with $KNH_2$ in supercritical ammonia at 873 K and 600 MPa yields a silicon nitride imide $Si_2N_2NH$, which is an intermediate compound during synthesis of $Si_3N_4$ by thermal decomposition of $Si(NH)_2$. Crystal growth and subsequent structure determination of $Si_2N_2NH$ succeeded after ammonothermal synthesis at 873 K and 600 MPa. In $Si_2N_2NH$ silicon is coordinated tetrahedrally by four N. The $SiN_4$ tetrahedra are connected via corners, resulting in layers of Si–N hexagons, which are linked by imide groups in prependicular direction [173]. Aditionnaly, in the system $Si/NH_3$, silicon imide $Si(NH)_2$ and silicon amide $Si(NH_2)_4$ are reported (see paragraph *Transition Metal, Group III and Group IV Metal Amides*). $Si(NH)_2$ is obtained from $SiCl_4$ in liquid ammonia at 353–363 K, however, up to now no crystal structure data is reported and the chemical nature of the compound is still unvertain. $Si(NH)_2$ serves as starting material for $Si_3N_4$ synthesis by thermal decomposition [179].

**Table 9.** Conditions for the ammonothermal synthesis of metal hydrides and hydride nitrides.

| Compound | Reactants Mineralizer | *T*/K | *p*/MPa | *t*/d | References |
|---|---|---|---|---|---|
| $ScH_2$ | Sc + $NH_4I$ | 773 | ≥11.3 | | [161] |
| $ZrH_{0.6}N$ | $ZrN(NH_2)$ | 633 | 600 | | [75] |
| $CeH_x$ ($x \leq 3$) | Ce | 395 | 400–500 | | [76] |
| $ThH_2$ | Th + Na/K | 473 | 500 | 7 | [33] |
| $ThHN_{1.23}$ | Th + $NH_4I$ | 573 | 355 | 10 | [33] |

### *5.5. Metal Hydrides and Nitride Hydrides*

In some systems, even metal hydrides can be synthesized prior the formation of the metal nitride is completed (see Table 9). This applies especially for the lighter lanthanides at temperatures below the formation temperature for the pure nitride. For example, $CeH_x$ with $x \leq 3$ was obtained next to CeN when pure cerium metal reacts with ammonia at 395 K and 400–500 MPa. The amount of hydrogen in $CeH_x$ ($x \leq 3$) decreases with increasing temperature, simultaneously the amount of CeN increases. At 475 K only pure CeN is obtained [76]. $ZrH_{0.6}N$ was obtained from $ZrN(NH_2)$ and $NH_3$ at 633 K and

600 MPa [75]. Only one compound is known from scandium under ammonothermal conditions, namely $ScH_2$. Scandium metal does not show any reaction up to 673 K. Using $NH_4I$ as mineralizer $ScH_2$ was obtained from scandium metal at 773 K [161].

### *5.6. Nitrides*

By the ammonothermal method nitride single crystals can be obtained at comparatively low temperatures $T \leq 700$ K [3] as can be seen in Table 10. The synthesis can be carried out in ammonobasic (e.g., EuN from Eu and K [122]), neutral (e.g., $Cu_3N$ from $[Cu(NH_3)_4]NO_3$ [20]) or ammonoacidic milieu (e.g., GaN + $NH_4I$ [62]). The formation process of the nitrides is not yet well understood (compare section *Crystallization Process*).

**Table 10.** Conditions for the ammonothermal synthesis of binary nitrides.

| Compound | Reactants + Mineralizer | *T*/K | *p*/MPa | *t*/d | Sample | References |
|---|---|---|---|---|---|---|
| $c$-$Be_3N_2$ | Be | 673 | 20.3 | 7 | m.c. | [2] |
| YN | Y + $NH_4I$ | 623 | 61 | 7 | m.c. | [163,174] |
| EuN | Eu + K 40:1 | 673 | 500 | 7 | s.c. | [122] |
| LaN | $K_3[La(NH_2)_6]$ + $KNH_2$ | 650 | 500 | 10 | s.c. | [3] |
| LaN | La + Na | 523–773 | 300–507 | 10 | s.c. | [3,131] |
| CeN | Ce + Cs | 490 | 200 | 12 | – | [159] |
| SmN | Sm + K | 433–453 | 500 | 10–30 | – | [121] |
| GdN | Gd + $NH_4I$ | 523 | 507 | 23 | – | [161] |
| GaN | Ga + $LiNH_2$/K | 823 | 500 | ≥7 | s.c. | [77] |
| GaN | GaN + $NH_4I$ | ≤1123 | ≤150 | – | s.c. | [62] |
| GaN | GaN + $KNH_2$ + KI | 673 | 240 | 7 | s.c. | [180] |
| $c$-GaN | $[Ga(NH)_{3/2}]_n$ + $NH_4I$ | 753 | – | 2–3 | s.c. | [181] |
| GaN:Mn | Ga + Mn + $KNH_2$ | 723–823 | 400–500 | 3–10 | s.c. | [182] |
| GaN:Cr | Ga + $CrBr_3$ + $KNH_2$ | 723–823 | 400–500 | 3–10 | s.c. | [182] |
| GaN:Fe | Ga + Fe + $LiNH_2$ | 723–773 | 400–500 | 3–10 | s.c. | [182] |
| AlN | Al + K | 723–873 | 200 | 1–18 | s.c | [78] |
| AlN | Al + $NH_4Cl$ | 723 | – | 2 | s.c | [11] |
| InN | In + $KNH_2$ | 723 | – | – | m.c. | [43] |
| $Fe_{4-x}Ni_xN$ | Fe + $FeI_2$ | 733–853 | 600–800 | – | s.c. | [183–185] |
| $\Theta$-$Mn_6N_{5+x}$ | $MnI_2$ + $NaNH_2$ | 673–723 | 600 | 60–120 | s.c. | [167] |
| $\eta$-$Mn_3N_2$ | Mn + $I_2$ or $MnI_2$ + $NaNH_2$ | 673–873 | 600 | 30 | s.c. | [167,186] |
| $\eta$-$Mn_3N_2$ | Mn + K/Rb | 673–873 | ≤600 | 35 | s.c. | [186] |
| $\epsilon$-$Mn_4N$ | Mn + GaN $A(1)NH_2$ | 723–823 | 400–500 | 3–10 | m.c. | [182] |
| $Ni_3N$ | $[Ni(NH_3)_6]Cl_2$ + $NaNH_2$ | 523 | 200 | 7 | s.c. | [187] |
| $Cu_3N$ | $[Cu(NH_3)_4]NO_3$ | 623–853 | ≥600 | – | s.c. | [20] |
| $Cu_3Pd_xN$ | $[Cu(NH_3)_4]NO_3$ + Cu | 723 | 600 | 7 | s.c. | [188] |
| $x = 0.020/0.989$ | + $[Pd(NH_3)_4](NO_3)_2$ | | | | | |

s.c. means single crystal, m.c. micro crystalline.

### 5.6.1. Alkaline-Earth Metal Nitrides

The first binary nitride synthesized by the ammonothermal method was $Be_3N_2$, which was obtained as pure cubic phase in 1966 by Juza and Jacobs from beryllium in supercritical ammonia at 673 K and 20.3 MPa [2]. In this way, the usual synthesis temperatures for beryllium nitride could be drastically reduced, since the reaction of beryllium to cubic beryllium nitride in ammonia flow requires temperatures of 1173–1373 K [189] and in nitrogen flow 1600 K [190]. Similar ammonothermal reaction conditions should apply for $Mg_3N_2$, although we are not aware of any publication describing a synthesis of $Mg_3N_2$ from supercritical ammonia. However, $Mg_3N_2$ decomposes at 633–648 K and 1 MPa in liquid ammonia to $Mg(NH_2)_2$ and at $T \geq 773$ K and $p \geq 5$ MPa to MgNH [115] (see paragraph *Imides, Nitride Imides, Nitride Amides and Amide Azides*). $\alpha$-$Be_3N_2$ crystallizes in the anti-bixbyite structure like $Mg_3N_2$, $\alpha$-$Ca_3N_2$ [190], $Cd_3N_2$ [191] and $Zn_3N_2$ [192]. It is not yet established, if the nitrides of strontium $Sr_3N_2$ and barium $Ba_3N_2$ can be synthesized, although the ternary nitrides $CaMg_2N_2$ and $SrMg_2N_2$ were reported [193]. The anti-bixbyite structure manifests the motif of a cubic closest packing of the nitrogen atoms, with the metal atoms occupying 75% of the tetrahedral holes in an ordered manner. Nitrogen is surrounded by distorted metal atom octahedra [190]. $\alpha$-$Be_3N_2$, $\beta$-$Be_3N_2$ [194], $Mg_3N_2$, $\alpha$-$Ca_3N_2$ [190] and $Zn_3N_2$ [195] are known to represent semiconductors. A decrease of the band gap value (obtained from experimental data) with increasing atomic weight is observed ($\alpha$-$Be_3N_2$: direct band gap of 3.8 eV [196], $Mg_3N_2$: 2.80 eV, $Ca_3N_2$: 1.55 eV [190] and $Zn_3N_2$ probably direct band gap of 1.01–1.25 eV [195,197]). Ammonothermal synthesis of nitrides with anti-bixbyite structure was only published for $\alpha$-$Be_3N_2$, nevertheless it is a promising method for bulk growth, especially since most of the other established synthesize routes only yield micro crystalline powders or films and no bulk material, which is necessary for many applications as semiconducting material. Additionally, due to its setup as transport growth, the ammonothermal method could lower the oxygen concentration, which is crucial for nitride semiconductors.

### 5.6.2. Group III and IV Nitrides

The nitrides of group III metals are considered very promising materials for optical devices in the short-wavelength region, high-frequency high-power electronics and fast-speed communication. Furthermore, they prove high physical and chemical endurance, which makes them attractive for applications in various settings. The use in optic and electronic devices stems back to their semiconducting nature. For example, GaN shows a wide direct bandgap of 3.39 eV [198], an electron mobility of $\sim$1500 $cm^2/Vs$ [36], a large critical breakdown electric field of $\sim$3 MV/cm and a saturation velocity of $\nu \leq 19$–$10^6$ cm/s. AlN and GaN find applications as blue lasers (e.g., for high capacity optical storage in CD-ROMs), in light emitting diodes, high electron mobility transistors and other devices [34,43]. The band gap for the group III nitrides decreases with increasing atomic weight of the metal constituent: AlN $E_g = 6.2$ eV at 295 K [199], GaN $E_g = 3.39$ eV [198] and InN $E_g = 0.7$–$0.8$ eV [200,201]. *h*-AlN, *h*-GaN and *h*-InN crystallize in the wurtzite-type structure (space group $P6_3mc$), where anions and cations are surrounded tetrahedrally by the respective counter ions.

For the growth of GaN or AlN for optoelectronic devices a feedstock setup is used, as described in paragraph *Reaction Vessels*(see Figure 6). This method allows the homo- and heteroepitaxial growth

of large single crystals. Both ammonobasic and ammonoacidic conditions are used for large scale syntheses, in which AlN [78] requires the highest growth temperatures and InN the lowest [43]. The ammonobasic method enables the growth of GaN wafers up to two inches in diameter [202] or bulk single crystals of 10 $mm^2$ by 1 mm thick [43] and dislocation density below $5 \cdot 10^4$ $cm^2$ [203]. Maximal growth rates of up to 40 µm/h (=960 µm/d) with rates of 10–30 µm/h (=240–720 µm/d) for all planes were reported [39]. *c*-GaN in a sphalerite structure (space group $F\bar{4}3m$) is also known and can be obtained from $[Ga(NH)_{3/2}]_x$ and $NH_4I$ under ammonothermal conditions (753 K) [181]. Indium nitride, like its lighter homologues, is an intriguing semiconducting material. Although, up to know research efforts are hindered by indium metal incorporations in as-grown InN, produced by decomposition of the thermodynamic instable InN, especially at temperatures above 723 K [204]. Similar structural defects provoked by formation of In particles are encountered in $In_xGa_{1-x}N$ solid solutions ($0 \leq x \leq 0.5$) [205], which are currently used in light-emitting and laser diodes. Their broad range of the direct band gap of $E_g$ = 0.77–1.75 eV allows to cover a spectral region from near-infrared to near-ultraviolet [206]. Due to the lower thermal stability of InN and its solid solutions with AlN and GaN, lower temperatures in synthesis and crystal growth are required. InN is supposed to be metastable at $T \geq 258$ K, kinetic constraints are believed to inhibit the decomposition at ambient conditions [207]. To our best knowledge, only once a synthesis of InN from ammonothermal conditions has been reported and has not yet been confirmed (see Table 10) [43]. However, the low temperatures and high pressures, which can be applied with the ammonothermal method, may be useful to stabilizes InN and its solid solutions without incorporation of In metal.

Doping of group III nitride semiconductors is used to enhance the emission range and *n*-type conductivity. The most frequently used donor dopant is silicon, but also rare-earth metal doping like with erbium was applied. On the other hand, unintentional doping, usually by oxygen contaminations, leads to reduced carrier concentrations and lower transparency [208]. Erbium doped GaN has shown emission of two erbium induced narrow green lines at 537 and 558 nm in the range of the visible spectrum, with the former one peaking at 300 K [209]. Doping of GaN with erbium under ammonothermal conditions manifests an infrared emission at 2.029 eV, due to intra-4*f* transitions, although no green transition was observed, probably due to the low erbium concentration ($1 \times 10^{18}$ $cm^{-3}$ for the Ga-polar growth, $1 \times 10^{17}$ $cm^{-3}$ for the N-polar growth). Additionally, erbium is discussed to work as getter for oxygen, crystallizing as erbium oxide nitride in the dissolution zone, thus lowering the oxygen concentration in the crystallization zone and consequently in the crystallized GaN. A lower concentration of Er and a higher impurity level (usually oxygen) in the nitrogen polar growth was observed, which is not surprising considering the different polarities of the seed crystal faces and the soluble species [210]. Furthermore, transition metals were used as dopants for GaN under ammonothermal conditions, yielding GaN:Mn (max. 1% Mn), GaN:Fe (max. 0.03% Fe), ferromagnetic GaN:Cr (max. 0.02% Cr) [182], GaN:Zn and GaN:Mg [211].

Cubic tin nitride $Sn_3N_4$ has been reported to form from $SnI_4$ or $SnBr_4$ with $KNH_2$ in liquid (but not supercritical) ammonia at 243 K followed by annealing in vacuo at 573 K [212].

### 5.6.3. Rare-Earth Metal Nitrides

Several rare-earth metal nitrides were obtained under ammonothermal conditions, namely YN [163,174], EuN [122], LaN [3,131], CeN [159], SmN [121] and GdN [161]. The reation conditions cover ammonoacidic and ammonobasic milieu, a temperature range from 433 (SmN) to 673 K (EuN) and pressures from 200 (CeN) to 507 MPa (EuN, LaN, SmN, GdN) (see Table 10). ScN, YN, LaN and GdN attract increasing research interest, since they are strongly suspected to be semiconductors, for ScN it even seems unequivocal [213]. Rare-earth metal nitrides cover a large range of properties, especially concerning their metallic or insulating character, CeN to GdN are considered half-metallic, TbN to HoN insulating and ErN to YbN metallic. GdN seems to play a special role, showing ferromagnetic properties with the Curie temperature in the range of $T_C$ = 58–69 K. The intricate physical and chemical properties of those nitrides stem back mainly to their partly filled 4*f* shells [214,215]. They crystallize in the rocksalt structure, with a six-fold coordination of $R^{3+}$ and $N^{3-}$ ions.

### 5.6.4. Transition Metal Nitrides

Transition metal nitrides manifest a vast number of interesting physical and chemical properties such as high hardness, mechanical strength, high melting point, magnetic and semiconducting properties [216]. For example, $\eta$-$Mn_3N_2$ exhibits an antiferromagnetic spin structure [167], $\epsilon$-$Mn_4N$ has a non-collinear ferrimagnetic spin-structure with a Curie temperature in the range of $T_C$ = 738–748 K [217,218], $\gamma'$-$Fe_4N$ is a ferromagnetic conductor with high thermal stability [219,220] and $Cu_3N$ is a diamagnetic semiconductor with an optical band gap of 0.8–1.9 eV [219,221]. The ammonothermal method so far yielded the following transition metal nitrides: $\Theta$-$Mn_6N_{5+x}$ [167], $\eta$-$Mn_3N_2$ [167,186], $\epsilon$-$Mn_4N$ [182], $Fe_{4-x}Ni_xN$ [183–185], $Ni_3N$ [187] and $Cu_3N$ [20]. From a supercritical ammonia-methanol mixture at 443–563 K and 16 MPa some nano crystalline nitrides were obtained, namely $Cr_2N$, $Co_2N$, $Fe_4N$, $Cu_3N$ and $Ni_3N$ [222].

The synthesis conditions for the above mentioned transition metal nitrides vary remarkably. The early 3*d*-transition metals are thermodynamically more stable than the later ones, which is manifested in the synthesis of the nitrides of Ti to Ni from the metals in supercritical nitrogen at ∼1800 K and 10,000 MPa. Yet, no copper nitrides were obtained from similar conditions [223], although the ammonothermal method in neutral conditions yields up to 10 mm·10 mm·2 mm $Cu_3N$ crystals [20]. The neutral milieu is applied by using $[Cu(NH_3)_4](NO_3)_2$ as mineralizer in the molar ratio 1:1 with Cu metal at 620–850 K and 300–800 MPa. The reaction proceeds by the comproportion of $[Cu(NH_3)_4](NO_3)_2$ with Cu metal to $[Cu(NH_3)_3]NO_3$, which subsequently forms $Cu_3N$ via $[Cu(NH_3)_2]NO_3$ [224]. The presence of $[Cu(NH_3)_2]NO_3$ crystals next to $Cu_3N$ in the product confirms this mechanism. The formation of pure $Cu_3N$ without any presence of oxides may surprise given the proposed reaction Equation (11) of nitrate to form water and elemental nitrogen.

$$3\,[Cu(NH_3)_4]NO_3 \rightarrow Cu_3N + 9\,H_2O + 4\,N_2 + 6\,NH_3 \quad (11)$$

However, the oxygen may be catched by the autoclave metal surface. $Cu_3N$ crystallizes in the anti-$ReO_3$-type structure, with nitrogen octahedrally surrounded by six Cu atoms and Cu forming collinear bonds with two nearest nitrogen atoms. The structure offers vacant sites, which can be

occupied, for example, by Cu (forming $Cu_4N$) or by Pd (e.g., forming $Cu_3Pd_xN$ [188]). Like $Cu_3N$ the ternary nitride $Cu_3Pd_xN$ ($x = 0.020/0.989$) is metastable at ambient temperature and can be obtained from Cu and $[Cu(NH_3)_2]NO_3$ in presence of $[Pd(NH_3)_4](NO_3)_2$ under ammonothermal conditions at 723 K and 600 MPa [188]. In contrast to semiconducting $Cu_3N$, the Pd doped variant exhibits metallic or semimetallic behavior [225].

Three different manganese nitrides could be obtained under ammonothermal conditions so far: $\Theta$-$Mn_6N_{5+x}$ and $\eta$-$Mn_3N_2$ from $MnI_2$ and $NaNH_2$ at 600 MPa and in temperature gradients from 673 K to 723 K and 673 K 873 K, respectively [167], $\epsilon$-$Mn_4N$ as by-product next to GaN:Mn during doping of GaN with Mn at 723–823 K and 400–500 MPa in ammonobasic milieu [182]. In $\eta$-$Mn_3N_2$ the Mn atoms form an *fcc* substructure with the N atoms occupying octahedral sites in such a way that perpendicular to [001] two fully occupied layers are followed by an empty one. Occupying all octahedral holes would lead to a rocksalt-type structure, like in the early transition and rare-earth metal nitrides [186]. $\Theta$-$Mn_6N_{5+x}$ realizes such a defect rocksalt structure, however, suffering a tetragonal distortion due to magnetostriction at ambient temperatures [226]. The structure of $\epsilon$-$Mn_4N$ also shows an *fcc* substructure of Mn atoms. Here the nitrogen atoms only occupy 1/4 of the octahedral voids in an ordered manner forming an inverse perovskite structure. Similar to the case of $Cu_3N$, one type of manganese atoms is coordinated linearly by two nitrogen atoms, a second type is exclusively surrounded by Mn of the first type [217].

$\gamma'$-$Fe_4N$ an isotype of $\epsilon$-$Mn_4N$, crystallizing in the inverse perovskite structure [183]. However, $\gamma'$-$Fe_4N$ obtained from supercritical ammonia [185] contained about 5 wt.% Ni ($Fe_{4-x}Ni_xN$) [183]. The nickel most likely origins from the autoclave wall, since the nickel based alloys used for autoclave manufacturing are corroded to a certain degree under ammonoacidic conditions. $Fe_{4-x}Ni_xN$ was obtained from Fe and $FeI_2$ at 733–853 K and 600–800 MPa.

$Ni_3N$ was synthesized ammonothermally from $[Ni(NH_3)_6]Cl_2$ and $NaNH_2$ at 523 K and 200 MPa in 7 days [187]. $Ni_3N$ crystallizes in the $\epsilon$-$Fe_3N$-type structure, with the Ni atoms realizing the motif of a hexagonal closed packing and the N atoms occupying corner-sharing octahedra. The Ni atoms are coordinated by two N atoms.

### *5.7. Non-Nitrogen Compounds*

Solvothermal methods allow crystal growth at comparatively low temperatures. Thus, oxides, carbonates, fluorides, sulfates and sulfide minerals such as proustite $Ag_3AsS_3$ can be grown under hydrothermal conditions [6]. However, use of water as solvent is prohibited in chemical synthesis and crystal growth if the target compound is water sensitive or forms stable solid hydrates. The ammonothermal technique in some cases proves superior even for formation of hydroxides, hydroxide hydrates, sulfides and hydrogen sulfides.

Alkali metal hydroxides, except LiOH, are difficult to grow as crystals suitable for single crystal X-ray diffraction, since they exist in different modifications in the range of ambient temperature to their melting point. Thus, the crystal growth from the melt is inhibited, while during growth from acqueous solution hydroxide hydrates are formed. The ammonothermal method allows the growth of single crystals of NaOH, KOH, RbOH [22] and CsOH [227] at conditions below the transition temperature of the

modification, which is stable at ambient conditions (see Table 11). Some alkali metal hydroxide hydrates were synthesized from ammonothermal synthesis as well. NaOH [22], $K(H_2O)OH$, $Rb(H_2O)OH$ [228] and $Cs(H_2O)OH$ [227] crystals were obtained by recrystallization of the micro crystalline substance in supercritical ammonia. The reaction of alkali metal hydroxide hydrates $A(1)(H_2O)OH$ ($A(1)$ = K, Rb, Cs) with alkali metal amides $A(1)NH_2$ ($A(1)$ = K, Rb, Cs) yields crystals of KOH, RbOH and CsOH [227]. This synthesis furnished the first crystallographic data of CsOH. $Ca(OH)_2$ can be obtained at 723 K and 69–207 MPa in one day from CaO and $NH_4I$ [57].

**Table 11.** Conditions for the ammonothermal synthesis of non-nitrogen compound crystals.

| Compound | Reactants + mineralizer | *T*/K | *p*/MPa | *t*/d | References |
|---|---|---|---|---|---|
| NaOH | NaOH | 523–473 | ≤600 | 10 | [22] |
| KOH | $K(H_2O)OH + KNH_2$ | ≤423 | ≤600 | ∼10 | [22] |
| RbOH | $Rb(H_2O)OH + RbNH_2$ | ≤365 | ≤600 | ∼10 | [22] |
| CsOH | $Cs(H_2O)OH + CsNH_2$ | 460 | 300 | 5 | [227] |
| CaOH | $CaO + NH_4I$ | 723 | 69–207 | 1 | [57,229] |
| $K(H_2O)OH$ | $K(H_2O)OH$ | 390–410 | 500 | 7–10 | [228] |
| $Rb(H_2O)OH$ | $Rb(H_2O)OH$ | 400–420 | 180 | 6 | [228] |
| $Cs(H_2O)OH$ | $Cs(H_2O)OH$ | 450 | 250 | 8 | [227] |
| LiHS | $LiNH_2 + H_2S$ | 300–370 | – | – | [3,230] |
| KHS | $KNH_2 + H_2S$ | 393 | ≤30 | 7 | [3,231] |
| CaS | $CaS + NH_4I$ | 573–673 | 69–207 | 1 | [57,229] |
| SrS | $SrS + NH_4I$ | 573–673 | 69–207 | 1 | [57,229] |
| CdS | $CdS + NH_4I$ | 573–673 | 69–207 | 1 | [57,229] |
| CuS | $CuI + CaS + NH_4I$ | 643 | 69–207 | 1 | [229] |
| $Cu_7S_4$ | $CuI + CaS + NH_4I$ | 643 | 69–207 | 1 | [229] |
| $CaCu_2S_2$ | $CuI + CaS + NH_4I$ | 573–673 | 69–207 | 1 | [57,229] |
| $NH_4Cu_4S_3$ | $CuI + CaS + NH_4I$ | 573–673 | 69–207 | 1 | [229] |
| $Na_2S_2$ | [a] | | | | [3,232] |
| $K_2S_2$ | [a] | | | | [3,232] |
| $Rb_2S_2$ | [a] | | | | [3,232] |
| $Cs_2S_2$ | Cs + Se | 573 | 200–300 | – | [21] |
| $Na_2S_3 \cdot NH_3$ | Na + S | 300–320 | 200 | – | [233] |
| $K_2S_3$ | K + S | 423 | 50 | – | [234] |
| $Rb_2S_3$ | Rb + S | 670 | 300 | – | [235] |
| $Cs_2S_3$ | Cs + S | 370 | 50 | – | [235] |
| $K_2S_5$ | [a] | | | | [3,232] |
| $Rb_2S_5$ | Rb + S | 450 | 5 | – | [236] |
| $Cs_2S_5$ | Cs + S | 323–373 | 10–200 | – | [237] |
| $Cs_2Se$ | Cs + Se | 573 | 200 | – | [3,238] |
| $Na_2Se_2$ | [a] | | | | [3,232] |

**Table 11.** *Cont.*

| Compound | Reactants + mineralizer | *T*/K | *p*/MPa | *t*/d | References |
|---|---|---|---|---|---|
| $K_2Se_2$ | [a] | | | | [3,232] |
| $Rb_2Se_2$ | [a] | | | | [3,232] |
| $Cs_2Se_2{\cdot}xNH_3$ | [a] | | | | [3,232] |
| $K_2Se_3$ | K + Se | 423 | 50 | – | [234] |
| $Rb_2Se_3$ | Rb + Se | 600 | 100 | – | [235] |
| $Cs_2Se_3$ | Cs + Se | 570 | 300 | – | [235] |
| $Rb_2Se_5$ | Rb + S | 450 | 500 | – | [236] |
| $K_2Te_3$ | [a] | | | | [3,232] |
| $Rb_2Te_3$ | Rb + Te | 500 | 100 | – | [239] |
| $Cs_2Te_3$ | Cs + Te | 500 | 100 | – | [239] |
| $Rb_2Te_5$ | Rb + Te | 473 | 200 | 7 | [56] |
| $Cs_2Te_5$ | Cs + Te | 473 | 200 | 90 | [240] |
| $K_2[CN_2]$ | Ga + K | 853 | 90 | – | [177] |

[a] No further information in literature.

For the synthesis of alkali metal hydrogen sulfides and selenides the common methods (e.g., molten metals or hydrogen sulfide hydrates in $H_2S$ stream, precipitation from a saturated solution) usually yield micro crystalline products. The application of liquid or supercritical ammonia in combination with $H_2S$ on alkali metal amides leads to well crystallized alkali metal hydrogen sulfide suitable for single crystal XRD, for example, LiHS and KHS (see Table 11) [3].

Micro crystalline metal sulfides CaS, SrS and CdS can be recrystallized in supercritical ammonia, using $NH_4I$ as mineralizer, at 573–673 K and 69–207 MPa in one day [57]. CuS, $Cu_7S_4$ and $NH_4Cu_4S_3$ were obtained at 573–673 K and 69–207 MPa as by-products during the synthesis of $CaCu_2S_2$ from CaS, CuI, $NH_4I$ in supercritical ammonia [229] (for details see Table 11).

Reactions of alkali metals with elemental chalcogens in supercritical or subcritical ammonia (e.g., $Cs_2S_5$ [237]) lead to various polychalcogenides of the types $A(1)_2E_2$ ($A(1)$ = Na, K, Rb, Cs; $E$ = S, Se, Te) and $A(1)_2E_5$ ($A(1)$ = Na, K, Rb, Cs; $E$ = S, Se) [3], namely, $Na_2S_3$ [233], $K_2S_3$ [234], $Rb_2S_3$ [235], $Cs_2S_3$ [235], $Cs_2S_5$ [237], $K_2Se_3$ [234], $Rb_2Se_3$ [235], $Cs_2Se_3$ [235], $Rb_2Te_3$ [239], $Cs_2Te_3$ [239], $Rb_2Te_5$ [56], $Cs_2Te_5$ [240]. Also, $Cs_2Se$ [3,238] and $Cs_2S_2$ [21] form under ammonothermal conditions and two alkali metal sulfide or selenide ammoniates were reported $Na_2S_3 \cdot NH_3$ [233] and $Cs_2Se_2{\cdot}xNH_3$ [3,232]. For the reaction conditions see Table 11. $Na_2S_3 \cdot NH_3$ [233], $Cs_2S_5$ [237] and $Rb_2S_5$ [236] were synthesized under subcritical conditions, but are mentioned for reasons of completeness. Although, some of those compounds were already known prior the introduction of ammonothermal synthesis in this field, a large number of structure determinations suceeded only thanks to single crystals grown from supercritical ammonia. In all mentioned polychalcogenides anions of the type $E_n^{2-}$ ($E$ = S, Se, Te, $n$ = 2–5) occur. There is a significant reduction of the distances between the anions of the type $E_n^{2-}$ ($E$ = S, Se, Te, $n$ = 2–6) in the alkali metal polychalcogenides osberved with increasing atomic weight of the chalcogen atom. This leads to extended anionic networks, e.g., in $RbTe_5$ and $CsTe_5$ [56].

Smaller complex anions occur in $K_2S_3$, $K_2Se_3$ [234], $Rb_2S_3$, $Rb_2Se_3$, $Cs_2S_3$, $Cs_2Se_3$ [235] and $Cs_2Te_3$ [239]. These compounds crystallize isoytpically in the $K_2S_3$-type structure and contain kinked $[S_3]^{2-}$ and $[Se_3]^{2-}$ anions, respectively. The alkali metal cations occupy 1/2 of trigonal prisms formed by four or five $[S_3]^{2-}$ or $[Se_3]^{2-}$ groups, resulting in a coordination number 1 + 6 for the cations, with one shorter (S/Se atom above plane of prism) and six larger distances (S/Se atoms in corners of the polyhedron) [234]. Interestingly, although $Cs_2Te_3$ crystallizes in the $K_2S_3$-type structure, $Rb_2Te_3$ crystallizes with the $K_2Te_3$-type structure [239]. Still, both structures contain $Te_3^{2-}$ polyanions. The reaction of alkali or alkaline-earth metals with carbon impurities under ammonothermal conditions leading to carbodiimides or cyanamides has already been discussed in paragraph *Imides, Nitride Imides, Nitride Amides and Amide Azides*. In this way $K_2[CN_2]$ was obtained as by-product during the synthesis of GaN from Ga and K metal with unintentional carbon impurities at 853 K and 90 MPa [177]. From a supercritical ammonia-methanol mixture at 443–563 K and 16 MPa some nano crystalline oxides were obtained, namely $Al_2O_3$, $TiO_2$ and $Ga_2O_3$ [222].

## 6. Conclusions

The ammonothermal synthesis is a useful technique suitable for various applications: for commercial large scale productions just as well as for small scale fundamental research. Its advantages for commercial applications are obviously the synthesis of bulk material even of difficult to crystallize compounds (for example, AlN and GaN), the high purity and low defect concentration of the products, due to the inherent chemical material transport, the comparatively mild conditions and the high scalability. For small scale fundamental research the method offers the crystal growth and stabilization of various materials, which are difficultly to crystallize by other synthesis routes, the decrease of reaction time compared to other methods and the access to new materials, which are not accessible by other methods. Nevertheless, the method has its limitations in temperature and pressure. The maximum temperature and pressure vary strongly, depending on the used reaction vessel design and material. Additionally, the corrosion of the autoclave material affects the purity of the products and the working lifetime of the autoclave. The use of a suitable liner material (e.g., precious metals, ceramics) can reduce the corrosion considerably and new constructions with inner heating and counter pressure allow the application of higher temperatures and pressures. Recent research reports indicate the suitability of the ammonothermal method in particular for commercial GaN crystal growth, due to competitive growth rates, high quality and high scalability. However, it is crucial for both the synthesis of novel materials and the improvement of the growth of large crystals to develop a fundamental comprehension of the physical and chemical processes during ammonothermal crystal growth. Knowledge about the thermodynamical and the chemical parameters will permit a specific and well-directed growth of novel functional materials.

The preparative possibilities of ammonothermal synthesis, more than fifty years after the beginning of development, are still far from exhausted. Tasks and future directions are manifold, starting from further exploration of new chemical compounds and materials synthesized by this technique including solid solutions and doped systems with potential for various applications. For this task a deeper understanding of the influence of starting materials, *i.e.*, nutrients for crystal growth as well as the

chemistry of the diverse mineralizers and co-mineralizers is badly needed. There is only little knowledge about dissolved species of the various constituents eventually forming the desired products under ammonobasic, ammononeutral and ammonoacidic conditions, depending on temperature, pressure and concentrations. This directly relates to the fundamental physical properties of the ammonia-based solutions of the mineralizers and dissolved materials, which will significantly deviate from those of pure ammonia, e.g., in terms of pressure-temperature relations. Similarly, more complex solutions, like, for example, buffer systems modifying the properties of the solvent with direct influence on the chemistry within the solution. Combined solvent systems as, e.g., ammonia-alcohol mixtures specially tailored for the desired products are a further completely open field, where scientists in the field just have scratched the surface of possibilities. The information on physical properties of ammonia-based solvents and chemistry in solution during the ammonothermal process will clearly lead to new directions of exploratory chemistry. Additionally, it will aid the improved mass-production of better semiconductor materials in sense of lower impurity and defect levels, enhanced growth rates of different crystallographic faces or even improved reactor design, due to a better understanding of dissolution, transport and material deposition processes including transport direction in the gradient and solubility of the desired material within the ammono-based solution. The latter point may lead to new concepts and combinations of nutrient, mineralizer, co-mineralizer and more complex solvent combinations. In terms of technical improvements, we will surely soon see novel liner materials and concepts as well as autoclaves for higher pressures or higher temperatures to be developed, in order to broaden the approachable range in synthetic chemistry and enhance the crystal growth process for commercial products. These commercial products in future may not only be restricted to *h*-GaN crystals, but be broadened to AlN, GaN-based solid solutions, further nitride-based materials and possibly even compounds not containing nitrogen. All in all, we see great prospects for solvothermal reactions in general, but for ammonothermal synthesis, crystal growth and materials production in particular.

## Acknowledgments

This work was funded by the Deutsche Forschungsgemeinschaft (DFG) within the frame of the research group FOR1600 “Chemie und Technologie der Ammonothermal-Synthese von Nitriden”. We thank all cooperation partners from FOR1600, in particular the group of Eberhard Schlücker and Nicolas Alt (Friedrich-Alexander Universität Erlangen-Nürnberg), without which our experimental work in this field would not be possible.

## Conflicts of Interest

The authors declare no conflicts of interest.

## References

1. Juza, R.; Jacobs, H.; Gerke, H. Ammonothermalsynthese von Metallamiden und Metallnitriden. *Ber. Bunsenges. Phys. Chem.* **1966**, *70*, 1103–1105.
2. Juza, R.; Jacobs, H. Ammonothermal synthesis of magnesium and beryllium amides. *Angew. Chem. Int. Ed.* **1966**, *5*, 247.

3. Jacobs, H.; Schmidt, D. High-pressure ammonolysis in solid-state chemistry. *Curr. Top. Mater. Sci.* **1982**, *8*, 387–427.
4. Byrappa, K.; Yoshimura, M. *Handbook of Hydrothermal Technology a Technology for Crystal Growth and Materials Processing*; Noyes Publications/Wiliam Andrew Publishing, LLC: Park Ridge, NY, USA, 2001.
5. Largeteau, A.; Darracq, S.; Goglio, G.; Demazeau, G. Solvothermal crystal growth of functional materials. *High Press. Res.* **2008**, *28*, 503–508.
6. Rabenau, A. The role of hydrothermal synthesis in preparative chemistry. *Angew. Chem. Int. Ed.* **1985**, *24*, 1026–1040.
7. Demazeau, G. Solvothermal reactions: An original route for the synthesis of novel materials. *J. Mater. Sci.* **2007**, *43*, 2104–2114.
8. Li, B.B.; Xie, Y.; Huang, J.; Qian, Y. Synthesis by a solvothermal route and characterization of $CuInSe_2$ nanowhiskers and nanoparticles. *Adv. Mater.* **1999**, *11*, 1456–1459.
9. Li, Y.D.; Duan, X.F.; Qian, Y.T.; Yang, L.; Ji, M.R.; Li, C.W. Solvothermal co-reduction route to the nanocrystalline III–V semiconductor InAs. *J. Am. Chem. Soc.* **1997**, *119*, 7869–7870.
10. Dwiliński, R.; Wysmolek, A.; Baranowski, J.; Kamińska, M.; Doradziński, R.; Jacobs, H. GaN synthesis by ammonothermal method. *Acta Phys. Pol. A* **1995**, *88*, 833–836.
11. Lan, Y.C.; Chen, X.L.; Cao, Y.G.; Xu, Y.P.; Xun, L.; Xu, T.; Liang, J.K. Low-temperature synthesis and photoluminescence of AlN. *J. Cryst. Growth* **1999**, *207*, 247–250.
12. Nicholas, N.J.; Franks, G.V.; Ducker, W.A. The mechanism for hydrothermal growth of zinc oxide. *CrystEngComm* **2012**, *14*, 1232–1240.
13. Nacken, R. Hydrothermale Mineralsynthese zur Züchtung von Quarzkristallen. *Chem. Ztg.* **1950**, *74*, 745–749.
14. Gleichmann, H.; Richert, H.; Hergt, R.; Barz, R.U.; Grassl, M. Hydrothermal liquid phase epitaxy of gallium orthophosphate on quartz crystal substrates. *Cryst. Res. Technol.* **2001**, *36*, 1181–1188.
15. Li, W.J.; Shi, E.W.; Chen, Z.Z.; Zhen, Y.Q.; Yin, Z.W. Solvothermal synthesis of superfine $Li_{1-x}Mn_2O_{4-\sigma}$ powders. *J. Solid State Chem.* **2002**, *163*, 132–136.
16. Vázquez-Vázquez, C.; López-Quintela, A.M. Solvothermal synthesis and characterisation of $La_{1-x}A_xMnO_3$ nanoparticles. *J. Solid State Chem.* **2006**, *179*, 3229–3237.
17. Bocquet, J.F.; Chhor, K.; Pommier, C. Barium titanate powders synthesis from solvothermal reaction and supercritical treatment. *Mater. Chem. Phys.* **1999**, *57*, 273–280.
18. Suchanek, W. Hydrothermal synthesis of alpha alumina ($\alpha$-$Al_2O_3$) powders: Study of the processing variables and growth mechanisms. *J. Am. Ceram. Soc.* **2010**, *93*, 399–412.
19. Korablov, S.; Yokosawa, K.; Korablov, D.; Tohji, K.; Yamasaki, N. Hydrothermal formation of diamond from chlorinated organic compounds. *Mater. Lett.* **2006**, *60*, 3041–3044.
20. Zachwieja, U.; Jacobs, H. Ammonothermalsynthese von Kupfernitrid, $Cu_3N$. *J. Less-Common Met.* **1990**, *161*, 175–184.
21. Böttcher, P. Zur Synthese und Struktur von $Cs_2S_2$. *J. Less-Common Met.* **1979**, *63*, 99–103.

22. Jacobs, H.; Kockelkorn, J.; Tacke, T. Hydroxide des Natriums, Kaliums und Rubidiums: Einkristallzüchtung und Röntgenographische Strukturbestimmung an der bei Raumtemperatur stabilen Modifikation. *Z. Anorg. Allg. Chem.* **1985**, *531*, 119–124.
23. Popolitov, V.; Litvin, B.; Lobachev, A. Hydrothermal crystallization of semiconducting compounds of group $A^{V}$ $B^{VI}$ $C^{VII}$ ($A^{V}$:Sb, Bi; $B^{VI}$:S, Se, Te; $C^{VII}$:I, Br, Cl). *Phys. Status Solidi A* **1970**, *3*, K1–K4.
24. Li, B.; Xie, Y.; Huang, J.; Su, H.; Qian, Y. A Solvothermal route to nanocrystalline $Cu_7Te_4$ at low temperature. *J. Solid State Chem.* **1999**, *146*, 47–50.
25. Lu, J.; Qi, P.; Peng, Y.; Meng, Z.; Yang, Z. Metastable MnS crystallites through solvothermal synthesis. *Chem. Mater.* **2001**, *13*, 2169–2172.
26. Hao, X.; Yu, M.; Cui, D.; Xu, X.; Wang, Q.; Jiang, M. The effect of temperature on the synthesis of BN nanocrystals. *J. Cryst. Growth* **2002**, *241*, 124–128.
27. Ramesha, K.; Seshadri, R. Solvothermal preparation of ferromagnetic sub-micron spinel $CuCr_2Se_4$ particles. *Solid State Sci.* **2004**, *6*, 841–845.
28. Kendall, J.L.; Canelas, D.A.; Young, J.L.; deSimone, J.M. Polymerizations in supercritical carbon dioxide. *Chem. Rev.* **1999**, *99*, 543–564.
29. Bunsen, R. Über die Spannkraft einiger condensirten Gase. *Ann. Phys.* **1839**, *46*, 97–103.
30. Bunsen, R. Bemerkungen zu einigen Einwürfen gegen mehrere Ansichten über die chemisch-geologischen Erscheinungen in Island. *Liebigs Ann.* **1848**, *65*, 70–85.
31. Schafhäutl, A. Die neuesten geologischen Hypothesen und ihr Verhältnis zur Naturwissenschaft überhaupt. *Gelehrte Anzeigen München* **1845**, *20*, 577.
32. De Sénarmont, M. Sur la formation des minéraux par voie humide dans les gites métallifères concrétionnés. *Ann. Chim. Phys.* **1851**, *32*, 129–175.
33. Blunck, H.; Juza, R. Verbindungen des Thoriums mit Stickstoff und Wasserstoff. *Z. Anorg. Allg. Chem.* **1974**, *410*, 9–20.
34. Akasaki, I. Nitride semiconductors–Impact on the future world. *J. Cryst. Growth* **2002**, *237-239*, 905–911.
35. Zhu, D.; Wallis, D.; Humphreys, C. Prospects of III-nitride optoelectronics grown on Si. *Rep. Progr. Phys.* **2013**, *76*, 106501.
36. Ehrentraut, D.; Meissner, E.; Bockowski, M. *Technology of Gallium Nitride Crystal Growth*; Springer Materials Sciences: Berlin Heidelberg, Germany, 2010.
37. Denis, A.; Goglio, G.; Demazeau, G. Gallium nitride bulk crystal growth processes: A review. *Mater. Sci. Eng. R.* **2006**, *R50*, 167–194.
38. Dwiliński, R.; Doradziński, R.; Garczyński, J.; Sierzputowski, L.; Puchalski, A.; Kanbara, Y.; Yagi, K.; Minakuchi, H.; Hayashi, H. Bulk ammonothermal GaN. *J. Cryst. Growth* **2009**, *311*, 3015–3018.
39. Ehrentraut, D.; Pakalapati, R.T.; Kamber, D.S.; Jiang, W.; Pocius, D.W.; Downey, B.C.; Mclaurin, M.; D'Evelyn, P.M. High quality, low cost ammonothermal bulk GaN substrates. *Jpn. J. Appl. Phys.* **2013**, *52*, 1–4.
40. Kim, E. Next Generation LED-SORAA. In Proceedings of Strategies in Light: Santa Clara Convention, Silicon Valley, CA, USA, 2 August 2012.

41. Letts, E. Development of GaN wafers for solid-state lighting via the ammonothermal method. In Proceedings of 8th International Workshop on Bulk Nitride Semiconductors, Seeon, Germany, 1 October 2013.
42. D'Evelyn, P.M.; Park, D.S.; LeBoeuf, S.F.; Rowland, L.B.; Narang, K.J.; Hong, H.; Arthur, S.D.; Sandvik, M. Gallium nitride crystals and wafers and method of making. US Patent 7,786,503 B2, 31 August 2010.
43. Wang, B.; Callahan, M. Ammonothermal synthesis of III-nitride crystals. *Cryst. Growth Des.* **2006**, *6*, 1227–1246.
44. Ehrentraut, D.; Sato, H.; Kagamitani, Y.; Sato, H.; Yoshikawa, A.; Fukuda, T. Solvothermal growth of ZnO. *Progr. Cryst. Growth Charact. Mater.* **2006**, *52*, 280–335.
45. Tomida, D.; Kagamitani, Y.; Bao, Q.; Hazu, K.; Sawayama, H.; Chichibu, S.F.; Yokoyama, C.; Fukuda, T.; Ishiguro, T. Enhanced growth rate for ammonothermal gallium nitride crystal growth using ammonium iodide mineralizer. *J. Cryst. Growth* **2012**, *353*, 59–62.
46. Bao, Q.; Saito, M.; Hazu, K.; Furusawa, K.; Kagamitani, Y.; Kayano, R.; Tomida, D.; Qiao, K.; Ishiguro, T.; Yokoyama, C.; *et al*. Ammonothermal crystal growth of GaN using an $NH_4F$ mineralizer. *Cryst. Growth Des.* **2013**, *13*, 4158–4161.
47. Holleman, A.; Wiberg, N.; Wiberg, E. *Lehrbuch der Anorganischen Chemie*, 102nd ed.; de Gruyter: Berlin, Germany, 2007.
48. Franklin, E.C.; Fernelius, W.C. *The Nitrogen System of Compounds*; Reinhold Publishing Corporation: New York, NY, USA, 1935.
49. Bronn, J. Über den Zustand der metallischen Lösungen. *Ann. Phys.* **1905**, *16*, 166–171.
50. Kraus, C.A. Solutions of metals in non-metallic solvents. VI. The conductance of the alkali metals in liquid ammonia. *J. Am. Chem. Soc.* **1921**, *43*, 749–770.
51. Haar, L.; Gallagher, J. Thermodynamic properties of ammonia. *J. Phys. Chem. Ref. Data* **1978**, *7*, 635–792.
52. Xiang, H.W. Vapor pressures, critical parameters, boiling points, and triple points of ammonia and trideuteroammonia. *J. Phys. Chem. Ref. Data* **2004**, *33*, 1005.
53. Lemmon, E.W.; McLinden, M.O.; Friend, D.G. Thermophysical properties of fluid systems, NIST standard reference data. Available online: http://webbook.nist.gov/chemistry/fluid/ (accessed on 09 December 2013).
54. Shatenshtein, A.I. A study of acid catalysis in liquid ammonia. *J. Am. Chem. Soc.* **1937**, *59*, 432–435.
55. Rondinini, S.; Longhi, P.; Mussini, P.R.; Mussini, T. Autoprotolysis constants in nonaqueous solvents and aqueous organic solvent mixtures. *Pure Appl. Chem.* **1987**, *59*, 1693–1702.
56. Böttcher, P.; Kretschmann, U. Darstellung und Kristallstruktur von Dirubidiumpentatellurid, $Rb_2Te_5$. *J. Less-Common Met.* **1983**, *95*, 81–91.
57. Purdy, A.P. Ammonothermal crystal growth of sulfide materials. *Chem. Mater.* **1998**, *10*, 692–694.
58. Glasser, L. Equations of state and phase diagrams of ammonia. *J. Chem. Educ.* **2009**, *86*, 1457–1458.

59. Alt, N.S.A.; Schlücker, E. Hochdruck-Sichtzelle für Untersuchungen des ammonothermalen Prozesses. *Chem. Ing. Tech.* **2011**, *83*, 280–285.
60. Alt, N.S.A.; Meissner, E.; Schlücker, E. Development of a novel in situ monitoring technology for ammonothermal reactors. *J. Cryst. Growth* **2012**, *350*, 2–4.
61. Hüttig, G.F. Apparat zur gleichzeitigen Druck- und Raummessung von Gasen (Tensi-eudiometer). *Z. Anorg. Allg. Chem.* **1920**, *114*, 161–173.
62. Yoshida, K.; Aoki, K.; Fukuda, T. High-temperature acidic ammonothermal method for GaN crystal growth. *J. Cryst. Growth* 2013, in press.
63. Callahan, M.J.; Chen, Q.S.C. Hydrothermal and Ammonothermal Growth of ZnO and GaN. In *Handbook of Crystal Growth*, 1st ed.; Dhanaraj, G., Byrappa, K., Prasad, V., Dudley, M., Eds.; Springer: Berlin/ Heidelberg, Germany, 2010; pp. 655–689.
64. Binnewies, M.; Glaum, R.; Schmidt, M.; Schmidt, P. *Chemical Vapor Transport Reactions*; Walter de Gruyter: Berlin, Germany & Boston, MA, USA, 2012.
65. Wang, B.; Callahan, M. Transport growth of GaN crystals by the ammonothermal technique using various nutrients. *J. Cryst. Growth* **2006**, *291*, 455–460.
66. Zhang, S.; Hintze, F.; Schnick, W.; Niewa, R. Intermediates in ammonothermal GaN crystal growth under ammonoacidic conditions. *Eur. J. Inorg. Chem.* **2013**, *2013*, 5387–5399.
67. Zhang, S.; Alt, N.S.A.; Schlücker, E.; Niewa, R. Novel alkali metal amidogallates as intermediates in ammonothermal GaN crystal growth. *J. Cryst. Growth* 2013, in press.
68. Alt, N.S.A.; Meissner, E.; Schlücker, E.; Frey, L. In situ monitoring technologies for ammonothermal reactors. *Phys. Status Solidi C* **2012**, *9*, 436–439.
69. Erlekampf, J.; Seebeck, J.; Savva, P.; Meissner, E.; Friedrich, J.; Alt, N.; Schlücker, E.; Frey, L. Numerical time-dependent 3D simulation of flow pattern and heat distribution in an ammonothermal system with various baffle shapes. *J. Cryst. Growth* 2014, in press.
70. Vogelsang, K.; Schröter, W.; Hoffmann, R.; Jacobs, H. Ein Beitrag zum Problem der Porenbildung. *Härterei Techn. Mitt.* **2002**, *57*, 42–48.
71. Cundy, C.S.; Cox, P.a. The hydrothermal synthesis of zeolites: Precursors, intermediates and reaction mechanism. *Microporous Mesoporous Mater.* **2005**, *82*, 1–78.
72. Moolenaar, R.J.; Evans, J.C.; McKeever, L.D. The structure of the aluminate ion in solutions at high pH. *J. Phys. Chem.* **1970**, *74*, 3629–3636.
73. Juza, R. Amides of the alkali and the alkaline earth metals. *Angew. Chem. Int. Ed.* **1964**, *3*, 471–481.
74. Juza, R. Über die Amide der 1. und 2. Gruppe des periodischen Systems. *Z. Anorg. Allg. Chem.* **1937**, *231*, 121–135.
75. Juza, R. Über ein Nitridamid des Zirkoniums. *Z. Anorg. Allg. Chem.* **1974**, *406*, 145–152.
76. Jacobs, H.; Kablitz, D. Untersuchung des Systems Kalium/Cer/Ammoniak. *Z. Anorg. Allg. Chem.* **1979**, *454*, 35–42.
77. Dwiliński, R.; Baranowski, J.; Kamińska, M. On GaN crystallization by ammonothermal method. *Acta Phys. Pol. A* **1996**, *90*, 763–766.
78. Peters, D. Ammonothermal synthesis of aluminum nitride. *J. Cryst. Growth* **1990**, *104*, 411–418.

79. Lan, Y.; Chen, X.L.; Xu, Y.; Cao, Y.; Huang, F. Syntheses and structure of nanocrystalline gallium nitride obtained from ammonothermal method using lithium metal as mineralizator. *Mater. Res. Bull.* **2000**, *35*, 2325–2330.
80. Guarino, R.; Rouxel, J. L'amidogallate de potassium $KGa(NH_2)_4$ et l'imidogallate $KGa(NH)_2$. L'obtention de l'amidure de gallium $Ga(NH_2)_3$. *Bull. Soc. Chim. Fr.* **1969**, *7*, 2284–2287.
81. Jacobs, H.; Nöcker, B. Neubestimmung von Struktur und Eigenschaften isotyper Natriumtetraamidometallate des Aluminiums und Galliums. *Z. Anorg. Allg. Chem.* **1993**, *619*, 381–386.
82. Molinié, P.; Brec, R.; Rouxel, J. Le pentaamidogallate de sodium: $Na_2Ga(NH_2)_5$. *C. R. Hebd. Seances Acad. Sci. C* **1972**, *274*, 1388–1391.
83. Ketchum, D.; Schimek, G.; Pennington, W.; Kolis, J. Synthesis of new group III fluoride–ammonia adducts in supercritical ammonia: Structures of $AlF_3(NH_3)_2$ and $InF_2(NH_2)(NH_3)$. *Inorg. Chim. Act.* **1999**, *294*, 200–206.
84. Jacobs, H.; Schröder, F.O. Penta-ammoniates of aluminium halide: The crystal structures of $AlX_3{\cdot}5NH_3$ with X = Cl , Br , I. *Z. Anorg. Allg. Chem.* **2002**, *628*, 951–955.
85. Johnson, W.C.; Parsons, J.B. Nitrogen compounds of gallium. *J. Phys. Chem.* **1932**, *36*, 2588–2594.
86. Wang, B.; Callahan, M.; Rakes, K.; Bouthillette, L.; Wang, S.Q.; Bliss, D.; Kolis, J. Ammonothermal growth of GaN crystals in alkaline solutions. *J. Cryst. Growth* **2006**, *287*, 376–380.
87. Ehrentraut, D.; Kagamitani, Y.; Yokoyama, C.; Fukuda, T. Physico-chemical features of the acid ammonothermal growth of GaN. *J. Cryst. Growth* **2008**, *310*, 891–895.
88. Purdy, A.P. Ammonothermal synthesis of cubic gallium nitride. *Chem. Mater.* **1999**, *11*, 1648–1651.
89. Peters, D.; Bock, J.; Jacobs, H. Hexaaminaluminiumiodidammoniakat-$[Al(NH_3)_6]I_3NH_3$-Darstellung und Kristallstruktur. *J. Less-Common Met.* **1989**, *154*, 243–250.
90. Jacobs, H.; Bock, J.; Stüve, C. Röntgenographische Strukturbestimmung und IR-spektroskopische Untersuchungen an Hexaamindiiodiden, $[M(NH_3)_6]I_2$, von Eisen und Mangan. *J. Less-Common Met.* **1987**, *134*, 207–214.
91. Leineweber, A.; Friedriszik, M.W.; Jacobs, H. Preparation and crystal structures of $Mg(NH_3)_2Cl_2$ , $Mg(NH_3)_2Br_2$, and $Mg(NH_3)_2I_2$. *J. Solid State Chem.* **1999**, *234*, 229–234.
92. Essmann, R. Influence of coordination on N-H...X- hydrogen bonds. Part 1. $[Zn(NH_3)_4]Br_2$ and $[Zn(NH_3)_4]I_2$. *J. Mol. Struct.* **1995**, *356*, 201–206.
93. Meyer, G.; Roos, M. Zwei Galliumfluorid-Ammoniakate: $Ga(NH_3)F_3$ und $Ga(NH_3)_2F_3$. *Z. Anorg. Allg. Chem.* **1999**, *625*, 1129–1134.
94. Bremm, S.; Meyer, G. Reactivity of ammonium halides: Action of ammonium chloride and bromide on iron and iron(III) chloride and bromide. *Z. Anorg. Allg. Chem.* **2003**, *629*, 1875–1880.
95. Bremm, S.; Meyer, G.; Möller, A.; Amann, P.; Sobotka, B. Einwirkung von Ammoniumhalogeniden auf Eisen und Eisenhalogenide. *Z. Anorg. Allg. Chem.* **2002**, *628*, 2190.

96. Widenmeyer, M.; Hansen, T.C.; Meissner, E.; Niewa, R. Formation and decomposition of iron nitrides observed by in situ powder neutron diffraction and thermal analysis. *Z. Anorg. Allg. Chem.* 2014, in press.
97. Hambley, T.W.; Lay, P.A. Comparisons of $\pi$-bonding and hydrogen bonding in isomorphous compounds: $[M(NH_3)_4Cl]Cl_2$ (M = Cr, Co, Rh, Ir, Ru, Os). *Inorg. Chem.* **1986**, *25*, 4553–4558.
98. Podberezskaya, N.; Yudanova, T.; Magarill, S.; Ipatova, E.; Romanenko, G.; Pervukhina, N.; Borisov, S. Structures of crystals of inorganic coordination compounds with complex ions $[MA_5X]$ and $[MX_5A]$ containing neutral (A) and acid (X) ligands, at very high packing densities. *J. Struct. Chem.* **1992**, *32*, 894–904.
99. Weishaupt, M.; Bezler, H.; Strähle, J. Darstellung und Kristallstruktur von $(NH_4)_2[V(NH_3)Cl_5]$. Die Kristallchemie der Salze $(NH_4)_2[V(NH_3)Cl_5]$, $[Rh(NH_3)Cl]Cl_2$ und $M_2VXCl_5$ mit M = K, $NH_4$, Rb, Cs und X = Cl, O. *Z. Anorg. Allg. Chem.* **1978**, *440*, 52–64.
100. Jacobs, H.; Schmidt, D.; Schmitz, D. Struktur und Eigenschaften der Caesiumamidolanthanat-monoammoniakate $Cs_3La(NH_2)_6{\cdot}NH_3$ und $Cs_4La(NH_2)_7{\cdot}NH_3$. *J. Less-Common Met.* **1981**, *81*, 121–133.
101. Pust, P.; Schmiechen, S.; Hintze, F.; Schnick, W. Ammonothermal synthesis and crystal structure of $BaAl_2(NH_2)_8{\cdot}2NH_3$. *Z. Anorg. Allg. Chem.* **2013**, *639*, 1185–1187.
102. Joannis, A. Sur l'amidure de sodium et sur un chlorure de disodammonium. *C. R. Hebd. Seances Acad. Sci. C* **1891**, *112*, 392–394.
103. Mammano, N.; Sienko, M. Low-temperature X-ray study of the compound tetraaminelithium. *J. Am. Chem. Soc.* **1968**, *90*, 6322–6324.
104. Kirschke, E.J.; Jolly, W.L. The reversibility of the reaction of alkali metals with liquid ammonia. *Inorg. Chem.* **1967**, *6*, 855–862.
105. Ruff, O.; Geisel, E. Über die Natur der sogenannten Metallammoniumverbindungen. *Ber. Dtsch. Chem. Ges.* **1906**, *39*, 828–843.
106. Juza, R.; Fasold, K.; Haeberle, C. Untersuchungen über die Amide der Alkalimetalle. *Z. Anorg. Allg. Chem.* **1937**, *234*, 75–85.
107. Juza, R.; Opp, K. Die Kristallstruktur des Lithiumamides. *Z. Anorg. Allg. Chem.* **1951**, *266*, 313–324.
108. Juza, R.; Weber, H.H.; Opp, K. Kristallstruktur des Natriumamids. *Z. Anorg. Allg. Chem.* **1956**, *284*, 73–82.
109. Jacobs, H.; Juza, R. Neubestimmung der Kristallstruktur des Lithiumamids. *Z. Anorg. Allg. Chem.* **1972**, *391*, 271–279.
110. Nagib, M.; Jacobs, H. Neutronenbeugung am Lithiumdeuteroamid. *Atomkernenergie* **1973**, *21*, 275–278.
111. Nagib, M.; Kistrup, H.; Jacobs, H. Neutronenbeugung am Natriumdeuteroamid. *Atomkernenergie* **1975**, *26*, 87–90.
112. Bohger, P.; Zeiske, T.; Jacobs, H. Neutronenbeugung an der Tieftemperaturmodifikation von Rubidiumdeuteroamid. *Z. Anorg. Allg. Chem.* **1998**, *624*, 364–366.

113. Nagib, M.; von Osten, E.; Jacobs, H. Röntgen- und Neutronenbeugung und Bestimmung der Wärmekapazität an Caesiumamid–$CsNH_2$–und Caesiumdeuteroamid–$CsND_2$–bei Temperaturen von 348 bis 33 K. *Atomkernenergie* **1983**, *43*, 47–54.
114. Jacobs, H.; Juza, R. Darstellung und Eigenschaften von Berylliumamid und -imid. *Z. Anorg. Allg. Chem.* **1969**, *370*, 248–253.
115. Jacobs, H.; Juza, R. Darstellung und Eigenschaften von Magnesiumamid und -imid. *Z. Anorg. Allg. Chem.* **1969**, *370*, 254–261.
116. Senker, J.; Jacobs, H.; Müller, M. Reorientational dynamics of amide ions in isotypic phases of strontium and calcium amide. 1. Neutron diffraction experiments. *J. Phys. Chem. B* **1998**, *102*, 931–940.
117. Nagib, M.; Jacobs, H.; Kistrup, H. Neutronenbeugung am Strontiumdeuteroamid, $Sr(ND_2)_2$, bei Temperaturen von 31 bis 570 K. *Atomkernenergie* **1979**, *33*, 38–42.
118. Jacobs, H.; Hadenfeldt, C. Die Kristallstruktur von Bariumamid, $Ba(NH_2)_2$. *Z. Anorg. Allg. Chem.* **1975**, *418*, 132–140.
119. Fröhling, B.; Kreiner, G.; Jacobs, H. Synthesis and crystal structure of manganese(II) and zinc amides, $Mn(NH_2)_2$ and $Zn(NH_2)_2$. *Z. Anorg. Allg. Chem.* **1999**, *625*, 211–216.
120. Hadenfeldt, C.; Gieger, B.; Jacobs, H. Die Kristallstruktur von Lanthanamid, $La(NH_2)_3$. *Z. Anorg. Allg. Chem.* **1974**, *410*, 104–112.
121. Jacobs, H.; Kistrup, H. Über das System Kalium/Samarium/Ammoniak. *Z. Anorg. Allg. Chem.* **1977**, *435*, 127–136.
122. Jacobs, H.; Fink, U. Untersuchung des Systems Kalium/Europium/Ammoniak. *Z. Anorg. Allg. Chem.* **1978**, *438*, 151–159.
123. Hadenfeldt, C.; Jacobs, H.; Juza, R. Über die Amide des Europiums und Ytterbiums. *Z. Anorg. Allg. Chem.* **1970**, *379*, 144–156.
124. Nagib, M.; von Osten, E.; Jacobs, H. Neutronenbeugung an drei Modifikationen des Kaliumdeuteroamids $KND_2$. *Atomkernenergie* **1977**, *29*, 41–47.
125. Nagib, M.; Jacobs, H.; von Osten, E. Neutronenbeugung am Kaliumdeuteroamid $KND_2$ bei 31 K. *Atomkernenergie* **1977**, *29*, 303–304.
126. Dachs, H. Bestimmung der Lage des Wasserstoffs in LiOH durch Neutronenbeugung. *Z. Kristallogr.* **1956**, *112*, 60–67.
127. Juza, R.; Jacobs, H.; Klose, W. Die Kristallstrukturen der Tieftemperaturmodifikationen von Kalium- und Rubidiumamid. *Z. Anorg. Allg. Chem.* **1965**, *338*, 171–178.
128. Jacobs, H.; Nagib, M.; Osten, E.V. Einkristallzüchtung und Kristallchemie der Alkali- und Erdalkalimetallamide. *Acta Crystallogr. A* **1978**, *34*, 168.
129. Schenk, P.; Tulhoff, H. Das System Kaliumamid/Ammoniak. *Angew. Chem.* **1962**, *74*, 962.
130. Juza, R.; Schumacher, H. Zur Kenntnis der Erdalkalimetallamide. *Z. Anorg. Allg. Chem.* **1963**, *324*, 278–286.
131. Jacobs, H.; Scholze, H. Untersuchung des Systems Na/La/$NH_3$. *Z. Anorg. Allg. Chem.* **1976**, *427*, 8–16.
132. Juza, R.; Fasold, K.; Kuhn, W. Untersuchungen über Zink- und Cadmiumamid. *Z. Anorg. Allg. Chem.* **1937**, *234*, 86–96.

133. Fitzgerald, F.F. Reactions in liquid ammonia. Potassium ammonozincate, cuprous nitride and an ammonobasic mercuric bromide. *J. Am. Chem. Soc.* **1907**, *29*, 656–665.
134. Joannis, M. Action du chlorure de bore sur le gaz ammoniac. *C. R. Hebd. Seances Acad. Sci.* **1902**, *135*, 1106.
135. Janik, J.F.; Wells, R.L. Gallium imide, $\{Ga(NH)_{3/2}\}_n$, a new polymeric precursor for gallium nitride powders. *Chem. Mater.* **1996**, *8*, 2708–2711.
136. Wiberg, E.; May, A. Über die Umsetzung von Aluminiumwasserstoff mit Ammoniak und Aminen. *Z. Naturforsch.* **1955**, *10b*, 229.
137. Semenenko, K.N.; Bulychev, B.M.; Shevlyagina, E.A. Aluminium hydride. *Russ. Chem. Rev. (Engl. Transl.)* **1966**, *35*, 649–658.
138. Purdy, A.P. Indium(III) amides and nitrides. *Inorg. Chem.* **1994**, *33*, 282–286.
139. Vigouroux, E.; Hugot, C. Silicon amide and imide. *C. R. Hebd. Seances Acad. Sci. C* **1903**, *136*, 1670–1672.
140. Glemser, O.; Naumann, P. Über den thermischen Abbau von Siliciumdiimid $Si(NH)_2$. *Z. Anorg. Allg. Chem.* **1959**, *298*, 134–141.
141. Molinié, P.; Brec, R.; Rouxel, J.; Herpin, P. Structures des amidoaluminates alcalins $MAl(NH_2)_4$ (M = Na, K, Cs). Structure de l'amidogallate de sodium $NaGa(NH_2)_4$. *Acta Crystallogr. B* **1973**, *29*, 925–934.
142. Drew, M.; Goulter, J.; Guémas-Brisseau, L.; Palvadeau, P.; Rouxel, J.; Herpin, P. Etude structurale d'amidobéryllates de rubidium et de potassium. *Acta Crystallogr. B* **1974**, *30*, 2579–2582.
143. Jacobs, H.; Jänichen, K. Lithiumaluminiumamid, $LiAl(NH_2)_4$, Darstellung, röntgenographische Untersuchung, Infrarotspektrum und thermische Zersetzung. *Z. Anorg. Allg. Chem.* **1985**, *531*, 125–139.
144. Tenten, A.; Jacobs, H. Strukturen und thermisches Verhalten von Kaliumtetraamidoaluminat, $\alpha$- und $\beta$-$KAl(NH_2)_4$. *Z. Kristallogr.* **1989**, *186*, 289–291.
145. Jacobs, H.; Harbrecht, B. Substitution in layers of cations in lithium amide: Potassium trilithium amide, $KLi_3(NH_2)_4$, and potassium heptalithium amide, $KLi_7(NH_2)_8$. *Z. Anorg. Allg. Chem.* **1984**, *518*, 87–100.
146. Kraus, F.; Korber, N. $K_2Li(NH_2)_3$ and $K_2Na(NH_2)_3$–Synthesis and crystal structure of two crystal-chemically isotypic mixed-cationic amides. *J. Solid State Chem.* **2005**, *178*, 1241–1246.
147. Jacobs, H.; Kockelkorn, J. Darstellung und Eigenschaften der Amidomagnesate des Kaliums und Rubidiums $K_2[Mg(NH_2)_4]$- und $Rb_2[Mg(NH_2)_4]$-Verbindungen mit isolierten $[Mg(NH_2)_4]^{2-}$ Tetraedern. *J. Less-Common Met.* **1984**, *97*, 205–214.
148. Jacobs, H.; Birkenbeul, J.; Schmitz, D. Strukturverwandschaft des Dicaesiumamidomagnesats, $Cs[Mg(NH_2)_4]$, zum $\beta$-$K_2SO_4$-Typ. *J. Less-Common Met.* **1982**, *85*, 79–86.
149. Jacobs, H.; Fink, U. Über Natrium- und Kaliumamidometallate des Calciums, Strontiums und Europiums. *J. Less-Common Met.* **1979**, *63*, 273–286.
150. Jacobs, H.; Kockelkorn, J.; Birkenbeul, J. Struktur und Eigenschaften der ternären Metallamide $NaCa(NH_2)_3$, $KBa(NH_2)_3$, $RbBa(NH_2)_3$, $Rb(Eu(NH_2)_3$ und $RbSr(NH_2)_3$. *J. Less-Common Met.* **1982**, *87*, 215–224.

151. Jacobs, H.; Fink, U. Darstellung und Kristallstruktur von $KCa(NH_2)_3$. *Z. Anorg. Allg. Chem.* **1977**, *435*, 137–145.
152. Jacobs, H.; Kockelkorn, J. Darstellung und Kristallstruktur des Rubdiumcalciumamids, $RbCa(NH_2)_3$. *Z. Anorg. Allg. Chem.* **1979**, *456*, 147–154.
153. Jacobs, H.; Kockelkorn, J. Über Caesiumamidometallate ($CsM(NH_2)_3$) des Calciums, Strontiums und Europiums; Verbindungen mit der Struktur "Hexagonaler Perowskite". *J. Less-Common Met.* **1981**, *81*, 143–154.
154. Jacobs, H. Darstellung und Eigenschaften des Caesiumbariumamids, $CsBa(NH_2)_3$: Strukturverwandschaft zum $NH_4CdCl_3$-Typ. *J. Less-Common Met.* **1982**, *85*, 71–78.
155. Hadenfeldt, C.; Gieger, B.; Jacobs, H. Darstellung und Kristallstruktur von $KLa_2(NH_2)_7$. *Z. Anorg. Allg. Chem.* **1974**, *408*, 27–36.
156. Hadenfeldt, C.; Gieger, B.; Jacobs, H. Darstellung und Kristallstruktur von $K_3La(NH_2)_6$. *Z. Anorg. Allg. Chem.* **1974**, *403*, 319–326.
157. Jacobs, H.; Stüve, C. Rubidiumhexaamidolanthanat und -neodymat, $Rb_3[La(NH_2)_6]$ und $Rb_3[Nd(NH_2)_6]$; Strukturverwandtschaft zu $K_3[Cr(OH_6)]$ und $K_4CdCl_6$. *Z. Anorg. Allg. Chem.* **1987**, *546*, 42–47.
158. Jacobs, H.; Schmidt, D. Über ein Caesiumheptaamidodilanthanat $CsLa_2(NH_2)_7$. *J. Less-Common Met.* **1981**, *78*, 51–59.
159. Jacobs, H.; Schmidt, D. Struktur und Eigenschaften von perowskitartigen Caesiumamidometallaten des Cers, Neodyms und Samariums $Cs_3Ln_2(NH_2)_9$. *J. Less-Common Met.* **1980**, *76*, 227–244.
160. Jacobs, H.; Kockelkorn, J. Über Kalium- und Rubidiumamidometallate des Europiums, Yttriums und Ytterbiums, $K_3M(NH_2)_6$ und $Rb_3M(NH_2)_6$. *J. Less-Common Met.* **1982**, *85*, 97–110.
161. Linde, G.; Juza, R. Amidometallate von Lanthan und Gadolinium und Umsetzung von Lanthan, Gadolinium und Scandium mit Ammoniak. *Z. Anorg. Allg. Chem.* **1974**, *409*, 191–198.
162. Jacobs, H.; Peters, D.; Hassiepen, K. Caesiumamidometallate des Gadoliniums, Ytterbiums und Yttriums mit perowskitverwandten Atomanordnungen $Cs_3M_2(NH_2)_9$. *J. Less-Common Met.* **1986**, *118*, 31–41.
163. Stuhr, A.; Jacobs, H.; Juza, R. Amide des Yttriums. *Z. Anorg. Allg. Chem.* **1973**, *395*, 291–300.
164. Peters, D.; Jacobs, H. Übergang von dichter Anionenpackung zu perowskitartiger Struktur bei Kalium- und Rubidiumamidyttriat, $KY(NH_2)_4$ und $RbY(NH_2)_4$. *J. Less-Common Met.* **1986**, *119*, 99–113.
165. Hadenfeldt, C.; Jacobs, H. Darstellung, Eigenschaften und Kristallstruktur von $Na_3[Yb(NH_2)_6]$. *Z. Anorg. Allg. Chem.* **1972**, *393*, 111–125.
166. Jacobs, H.; Jänichen, K. Darstellung und Kristallstruktur von Tetraamidoaluminaten des Rubidiums und Caesiums, $Rb[Al(NH_2)_4]$ und $Cs[Al(NH_2)_4]$. *J. Less-Common Met.* **1990**, *159*, 315–325.
167. Kreiner, G.; Jacobs, H. Magnetische Struktur von $\eta$-$Mn_3N_2$. *J. Alloys Compd.* **1992**, *183*, 345–362.

168. Richter, T.M.M.; Zhang, S.; Niewa, R. Ammonothermal synthesis of dimorphic $K_2[Zn(NH_2)_4]$. *Z. Kristallogr.* **2013**, *228*, 351–358.
169. Fröhling, B.; Jacobs, H. Positions of the protons in potassium tetraamidozincate, $K_2Zn(NH_2)_4$. *Z. Anorg. Allg. Chem.* **1997**, *623*, 1103–1107.
170. Brec, R.; Novak, A.; Rouxel, J. Etude par spectroscopie infrarouge des amidoaluminates de lithium, sodium et potassium. *Bull. Soc. Chim. Fr.* **1967**, *7*, 2432–2435.
171. Drew, M.; Guémas, L.; Chevalier, P.; Palvadeau, P.; Rouxel, J. Etude structurale de l'amidozincate de rubidium $Rb_2Zn(NH_2)_4$ et de l'amidomanganite de potassium $K_2Mn(NH_2)_4$. *Rev. Chim. Min.* **1975**, *12*, 419–426.
172. Jacobs, H.; Gieger, B.; Hadenfeldt, C. Über das System Kalium/Lanthan/Ammoniak. *J. Less-Common Met.* **1979**, *64*, 91–99.
173. Peters, D.; Jacobs, H. Ammonothermalsynthese von kristallinem Siliciumnitridimid, $Si_2N_2NH$. *J. Less-Common Met.* **1989**, *146*, 241–249.
174. Harbrecht, B.; Jacobs, H. Hochdrucksynthese von Caesiumamidazid, $Cs_2(NH_2)N_3$ aus Caesiummetall und Ammoniak. *Z. Anorg. Allg. Chem.* **1983**, *500*, 181–187.
175. Höhn, P.; Kniep, R.; Maier, J. $Ba_9N[N_3][TaN_4]_2$ ein Nitridotantalat(V) mit Nitrid- und Azid-Ionen. *Angew. Chem.* **1993**, *105*, 1409–1410.
176. Clarke, S.J.; DiSalvo, F.J. Crystal structure of nonabarium bis(tetranitridoniobate) nitride azide, $Ba_9[NbN_4]_2N[N_3]$. *Z. Kristallogr. NCS* **1997**, *212*, 309–310.
177. Zhang, S.; Zherebtsov, D.; DiSalvo, F.J.; Niewa, R. $Na_5[CN_2]_2[CN]$, $(Li,Na)_5[CN_2]_2[CN]$, and $K_2[CN_2]$: Carbodiimides from high-pressure synthesis. *Z. Anorg. Allg. Chem.* **2012**, *638*, 2111–2116.
178. Stock, A.; Blix, M. Über das Borimid, $B_2(NH)_3$. *Ber. Dtsch. Chem. Ges.* **1901**, *34*, 3039–3048.
179. Blix, M.; Wirbelauer, W. Über das Siliciumsulfochlorid, $SiSCl_2$, Siliciumimid, $Si(NH)_2$, Siliciumstickstoffimid (Silicam), $Si_2N_3H$ und den Siliciumstickstoff, $Si_3N_4$. *Ber. Dtsch. Chem. Ges.* **1903**, *36*, 4220–4228.
180. Ketchum, D.; Kolis, J. Crystal growth of gallium nitride in supercritical ammonia. *J. Cryst. Growth* **2001**, *222*, 431–434.
181. Jouet, R.J.; Purdy, A.P.; Wells, R.L.; Janik, J.F. Preparation of phase pure cubic gallium nitride, *c*-GaN, by ammonothermal conversion of gallium imide, $\{Ga(NH)_{3/2}\}_n$. *J. Clust. Sci.* **2002**, *13*, 469–486.
182. Zajac, M.; Gosk, J.; Grzanka, E.; Stelmakh, S.; Palczewska, M.; Wysmoek, A.; Korona, K.; Kamiska, M.; Twardowski, A. Ammonothermal synthesis of GaN doped with transition metal ions (Mn, Fe, Cr). *J. Alloys Compd.* **2008**, *456*, 324–338.
183. Jacobs, H.; Rechenbach, D.; Zachwieja, U. Structure determination of $\gamma$'-$Fe_4N$ and $\epsilon$-$Fe_3N$. *J. Alloys Compd.* **1995**, *227*, 10–17.
184. Jacobs, H.; Rechenbach, D.; Zachwieja, D. Untersuchungen zur Struktur und zum Zerfall von Eisennitriden- $\gamma$'-$Fe_4N$ und $\epsilon$-$Fe_3N$. *Härterei Techn. Mitt.* **1995**, *50*, 205–213.
185. Jacobs, H.; Bock, J. Einkristallzüchtung von $\gamma'$-$Fe_4N$ in überkritischem Ammoniak. *J. Less-Common Met.* **1987**, *134*, 215–220.

186. Jacobs, H.; Stüve, C. Hochdrucksynthese der $\eta$-phase im System Mn-N: $Mn_3N_2$. *J. Less-Common Met.* **1984**, *96*, 323–329.
187. Leineweber, A.; Jacobs, H.; Hull, S. Ordering of nitrogen in nickel nitride $Ni_3N$ determined by neutron diffraction. *Inorg. Chem.* **2001**, *40*, 5818–5822.
188. Jacobs, H.; Zachwieja, U. Kupferpalladiumnitride, $Cu_3Pd_xN$ mit $x = 0,020$ und 0,989, Perowskite mit "bindender $3d^{10}$-$4d^{10}$-Wechselwirkung". *J. Less-Common Met.* **1991**, *170*, 185–190.
189. von Stackelberg, M.; Paulus, R. Untersuchungen über die Kristallstrukturen der Nitride und Phosphide zweiwertiger Metalle. *Z. Physik. Chem. B* **1933**, *22*, 305.
190. Reckeweg, O.; Lind, C.; DiSalvo, F.J. Rietveld refinement of the crystal structure of $\alpha$-$Be_3N_2$ and the experimental determination of optical band gaps for $Mg_3N_2$, $Ca_3N_2$ and $CaMg_2N_2$. *Z. Naturforsch.* **2003**, *58b*, 159–162.
191. Karau, F.; Schnick, W. Synthese von Cadmiumnitrid $Cd_3N_2$ durch thermischen Abbau von Cadmiumazid $Cd(N_3)_2$ und Kristallstrukturbestimmung aus Röntgen-Pulverbeugungsdaten. *Z. Anorg. Allg. Chem.* **2007**, *633*, 223–226.
192. Partin, D.E.; Williams, D.J.; O'Keeffe, M. The crystal structures of $Mg_3N_2$ and $Zn_3N_2$. *J. Solid State Chem.* **1997**, *132*, 56–59.
193. Reckeweg, O.; DiSalvo, F.J. About binary and ternary alkaline earth metal nitrides. *Z. Anorg. Allg. Chem.* **2001**, *627*, 371–377.
194. Soto, G.; Diaz, J.A.; De la Cruz, W.; Contreras, O.; Moreno, M.; Reyes, A. Epitaxial $\alpha$-$Be_3N_2$ thin films grown on Si substrates by reactive laser ablation. *Mater. Sci. Eng., B.* **2002**, *94*, 62–65.
195. García Núñez, C.; Pau, J.; Hernández, M.; Cervera, M.; Ruiz, E.; Piqueras, J. On the zinc nitride properties and the unintentional incorporation of oxygen. *Thin Solid Films* **2012**, *520*, 1924–1929.
196. Soto, G.; Díaz, J.A.; Machorro, R.; Reyes-Serrato, A.; de la Cruz, W. Beryllium nitride thin film grown by reactive laser ablation. *Mater. Lett.* **2002**, *52*, 29–33.
197. Toyoura, K.; Tsujimura, H.; Goto, T.; Hachiya, K.; Hagiwara, R.; Ito, Y. Optical properties of zinc nitride formed by molten salt electrochemical process. *Thin Solid Films* **2005**, *492*, 88–92.
198. Maruska, H.P.; Tietjen, J.J. The preparation and properties of vapor-deposited single-crystalline GaN. *Appl. Phys. Lett.* **1969**, *15*, 327.
199. Perry, P.B.; Rutz, R.F. The optical absorption edge of single-crystal AlN prepared by a close-spaced vapor process. *Appl. Phys. Lett.* **1978**, *33*, 319–321.
200. Wu, J.; Walukiewicz, W.; Shan, W.; Yu, K.; Ager, J.; Haller, E.E.; Lu, H.; Schaff, W.J. Effects of the narrow band gap on the properties of InN. *Phys. Rev. B* **2002**, *66*, 201403.
201. Xie, R.J.; Bert Hintzen, H.T. Optical properties of (oxy)nitride materials: A review. *J. Am. Ceram. Soc.* **2013**, *96*, 665–687.
202. Dwiliński, R.; Doradziński, R.; Garczyński, J.; Sierzputowski, L.; Kucharski, R.; Zajac, M.; Rudziński, M.; Kudrawiec, R.; Serafińczuk, J.; Strupiński, W. Recent achievements in AMMONO-bulk method. *J. Cryst. Growth* **2010**, *312*, 2499–2502.

203. Gogova, D.; Petrov, P.P.; Buegler, M.; Wagner, M.R.; Nenstiel, C.; Callsen, G.; Schmidbauer, M.; Kucharski, R.; Zajac, M.; Dwiliński, R.; *et al.* Structural and optical investigation of non-polar (1–100) GaN grown by the ammonothermal method. *J. Appl. Phys.* **2013**, *113*, 203513.
204. Shubina, T.; Ivanov, S.; Jmerik, V.; Solnyshkov, D.; Vekshin, V.; Kopev, P.; Vasson, A.; Leymarie, J.; Kavokin, A.; Amano, H.; *et al.* Mie resonances, infrared emission, and the band gap of InN. *Phys. Rev. Lett.* **2004**, *92*, 117407.
205. Komissarova, T.A.; Jmerik, V.N.; Ivanov, S.V.; Paturi, P. Detection of metallic in nanoparticles in InGaN alloys. *Appl. Phys. Lett.* **2011**, *99*, 072107.
206. Wu, J.; Walukiewicz, W.; Yu, K.M.; Ager, J.W.; Haller, E.E.; Lu, H.; Schaff, W.J. Small band gap bowing in $In_{1-x}Ga_xN$ alloys. *Appl. Phys. Lett.* **2002**, *80*, 4741.
207. Ranade, M.R.; Tessier, F.; Navrotsky, A.; Marchand, R. Calorimetric determination of the enthalpy of formation of InN and comparison with AlN and GaN. *J. Mater. Res.* **2011**, *16*, 2824–2831.
208. Richter, E.; Stoica, T.; Zeimer, U.; Netzel, C.; Weyers, M.; Tränkle, G. Si doping of GaN in hydride vapor-phase epitaxy. *J. Electron. Mater.* **2013**, *42*, 820–825.
209. Steckl, A.J.; Birkhahn, R. Visible emission from Er-doped GaN grown by solid source molecular beam epitaxy. *Appl. Phys. Lett.* **1998**, *73*, 1700–1702.
210. Adekore, B.T.; Callahan, M.J.; Bouthillette, L.; Dalmau, R.; Sitar, Z. Synthesis of erbium-doped gallium nitride crystals by the ammonothermal route. *J. Cryst. Growth* **2007**, *308*, 71–79.
211. Korona, K.P.; Doradziński, R.; Palczewska, M.; Pietras, M.; Kamiska, M.; Kuhl, J. Properties of zinc acceptor and exciton bound to zinc in ammonothermal GaN. *Phys. Status Solidi B* **2003**, *235*, 40–43.
212. Scotti, N.; Kockelmann, W.; Senker, J. $Sn_3N_4$, a Tin(IV) nitride–syntheses and the first crystal structure determination of a binary tin-nitrogen compound. *Z. Anorg. Allg. Chem.* **1999**, *625*, 1435–1439.
213. Louhadj, A.; Ghezali, M.; Badi, F.; Mehnane, N.; Cherchab, Y.; Amrani, B.; Abid, H.; Sekkal, N. Electronic structure of ScN, YN, LaN and GdN superlattices. *Superlatt. Microstruct.* **2009**, *46*, 435–442.
214. Srivastava, V.; Rajagopalan, M.; Sanyal, S.P. Theoretical investigation on structural, magnetic and electronic properties of ferromagnetic GdN under pressure. *J. Magn. Magn. Mater.* **2009**, *321*, 607–612.
215. Li, D.X.; Haga, Y.; Shida, H.; Suzuki, T. Magnetic properties of ferromagnetic GdN. *Physica B* **1994**, *199/200*, 631–633.
216. Mancera, L.; Rodr, J.A. First principles calculations of the ground state properties and structural phase transformation in YN. *J. Phys.: Condens. Matter* **2003**, *15*, 2625–2633.
217. Niewa, R. Nitridocompounds of manganese: Manganese nitrides and nitridomanganates. *Z. Kristallogr.* **2002**, *217*, 8–23.
218. Takei, W.J.; Heikes, R.R.; Shirane, G. Magnetic structure of $Mn_4N$-type compounds. *Phys. Rev. B* **1962**, *125*, 1893–1897.

219. Borsa, D.M.; Grachev, S.; Presura, C.; Boerma, D.O. Growth and properties of $Cu_3N$ films and $Cu_3N/\gamma$'-$Fe_4N$ bilayers. *Appl. Phys. Lett.* **2002**, *80*, 1823–1825.
220. Sakuma, A. Self-consistent calculations for the electronic structures of iron nitrides, $Fe_3N$, $Fe_4N$ and $Fe_{16}N_2$. *J. Magn. Magn. Mater.* **1991**, *102*, 127–134.
221. Wang, D.Y. Properties of various sputter-deposited CuN thin films. *J. Vac. Sci. Technol. A* **1998**, *16*, 2084–2092.
222. Desmoulins-Krawiec, S.; Aymonier, C.; Loppinet-Serani, A.; Weill, F.; Gorsse, S.; Etourneau, J.; Cansell, F. Synthesis of nanostructured materials in supercritical ammonia: nitrides, metals and oxides. *J. Mater. Chem.* **2004**, *14*, 228–232.
223. Hasegawa, M.; Yagi, T. Systematic study of formation and crystal structure of 3d-transition metal nitrides synthesized in a supercritical nitrogen fluid under 10 GPa and 1800 K using diamond anvil cell and YAG laser heating. *J. Alloys Compd.* **2005**, *403*, 131–142.
224. Zachwieja, U.; Jacobs, H. Kolumnarstrukturen bei Tri- und Diamminnitraten, $[M(NH_3)_3]NO_3$ und $[M(NH_3)_2]NO_3$ des einwertigen Kupfers und Silbers. *Z. Anorg. Allg. Chem.* **1989**, *571*, 37–50.
225. Hahn, U.; Weber, W. Electronic structure and chemical-bonding mechanism of $Cu_3N$, $Cu_3NPd$, and related Cu(I) compounds. *Phys. Rev. B: Condens. Matter* **1996**, *53*, 12684–12693.
226. Leineweber, A.; Niewa, R.; Jacobs, H.; Kockelmann, W. The manganese nitrides $\eta$-$Mn_3N_2$ and $\Theta$-$Mn_6N_{5+x}$: Nuclear and magnetic structures. *J. Mater. Chem.* **2000**, *10*, 2827–2834.
227. Jacobs, H.; Harbrecht, B. Eine neue Darstellungsmethode für Caesiumhydroxid. *Z. Naturforsch.* **1981**, *36b*, 270–271.
228. Jacobs, H.; Tacke, T.; Kockelkorn, J. Hydroxidmonohydrate des Kaliums und Rubidiums; Verbindungen, deren Atomanordnungen die Schreibweise $K(H_2O)OH$ bzw. $Rb(H_2O)OH$ nahelegen. *Z. Anorg. Allg. Chem.* **1984**, *516*, 67–78.
229. Purdy, A.P. Ammonothermal growth of chalcogenide single crystal materials. US Patent 5,902,396, 11 May 1999.
230. Jacobs, H.; Kirchgässner, R.; Bock, J. Darstellung und Kristallstruktur von Lithiumhydrogensulfid LiHS. *Z. Anorg. Allg. Chem.* **1989**, *569*, 111–116.
231. Jacobs, H.; Erten, C. Über Kaliumhydrogensulfid, KHS. *Z. Anorg. Allg. Chem.* **1981**, *473*, 125–132.
232. Böttcher, P. Beiträge zur Kenntnis der Alkalimetallpolychalkogenide. Habilitation Thesis, RWTH Aachen, Germany, 1980.
233. Böttcher, P. Zur Kenntnis der Verbindung $Na_2S_3$. *Z. Anorg. Allg. Chem.* **1980**, *467*, 149–157.
234. Böttcher, P. Die Kristallstruktur von $K_2S_3$ und $K_2Se_3$. *Z. Anorg. Allg. Chem.* **1977**, *432*, 167–172.
235. Böttcher, P. Preparation and crystal structure of the dialkali metal trichalcogenides $Rb_2S_3$, $Rb_2Se_3$ and $Cs_2Se_3$. *Z. Anorg. Allg. Chem.* **1980**, *461*, 13–21.
236. Böttcher, P. Synthesis and crystal structure of the dirubidiumpentachalcogenides $Rb_2S_5$ and $Rb_2Se_5$. *Z. Kristallogr.* **1979**, *150*, 65–73.
237. Böttcher, P.; Kruse, K. Darstellung und Kristallstruktur von Dicaesiumpentasulfid ($Cs_2S_5$). *J. Less-Common Met.* **1982**, *83*, 115–125.

238. Böttcher, P. Zur Kenntnis von $Cs_2Se$. *J. Less-Common Met.* **1980**, *76*, 271–277.
239. Böttcher, P. Synthesis and crystal structure of $Rb_2Te_3$ and $Cs_2Te_3$. *J. Less-Common Met.* **1980**, *70*, 263–271.
240. Böttcher, P. Darstellung und Kristallstruktur von Dicaesiumpentatellurid, $Cs_2Te_5$. *Z. Anorg. Allg. Chem.* **1982**, *491*, 39–46.